RESEARCH ARTICLE

VOLCANICA

Offshore evidence for volcanic landslide post Last Glacial Maximum at sub-Antarctic Heard Island, southern Indian Ocean

Jodi M. Fox[α,β], Sally J. Watson*[γ,δ], Trevor J. Falloon[ε], Rebecca J. Carey[ε], Joanne M. Whittaker[α], Erica A. Spain[γ], Robert A. Duncan[ζ], Richard J. Arculus[η], and Millard F. Coffin[α,θ,ι]

[α] Institute for Marine and Antarctic Studies, University of Tasmania, Hobart, Australia.
[β] National Museum of Nature and Science, Tsukuba, Japan.
[γ] National Institute of Water and Atmospheric Research, Wellington, New Zealand.
[δ] Institute of Marine Science, University of Auckland, Auckland, New Zealand.
[ε] Centre for Ore Deposits and Earth Science, University of Tasmania, Hobart, Australia.
[ζ] College of Earth, Ocean, and Atmospheric Sciences, Oregon State University, Corvallis, OR 97331, USA.
[η] Research School of Earth Sciences, Australian National University, Canberra, Australia.
[θ] School of Earth and Climate Sciences, University of Maine, Orono, ME 04469, USA.
[ι] Geology and Geophysics, Woods Hole Oceanographic Institution, Woods Hole, MA 02543, USA.

Abstract

Heard Island, an active sub-Antarctic intraplate volcanic island on the Kerguelen Plateau, is mostly covered by glaciers. The amphitheatre shaped summit of the active volcanic centre, Big Ben (2813 m), has been interpreted to be the product of a significant volcanic landslide. Here we present the first offshore geomorphological and geological evidence supporting a volcanic landslide on Big Ben, including: (1) the seafloor to the southwest of Heard resembling a landslide deposit, covering at least 467 km^2, (2) the spatial correlation between the onshore landslide scar and the offshore deposit and (3) the consistency in lithologies and compositions of rocks sampled from the deposit with the onshore *in situ* lithologies. ^{40}Ar/^{39}Ar geochronology constrains the maximum age of the volcanic landslide to 18.0 ± 1.4 ka, post the Last Glacial Maximum. Finally, we assess the risk of volcanic landslide at Heard Island in the future.

Keywords: Sector collapse; Kerguelen; Intraplate; Glacier; Debris avalanche; 40Ar/39Ar.

1 Introduction

Volcanic landslides can be catastrophic events in the life cycle of volcanic islands, influencing the island morphology (e.g. Piton de la Fournaise, La Réunion [Labazuy 1996]), lava composition (e.g. Tenerife, Canary Islands [Carracedo et al. 2010]), and volcanic plumbing systems (e.g. Fogo, Cape Verde [Watt 2019]). A range of terminology has been used in the literature to describe landslides on the flanks of volcanoes (e.g. sector collapse, lateral collapse, flank collapse, slope failure, and flank failure) and their deposits [Siebert 1984; Glicken 1991; Bernard et al. 2021]. Here we use the descriptive terminology of Bernard et al. [2021] who defined a volcanic landslide as the rapid, translation of multiple volcanic units over a slide surface, produced by the failure of a portion or portions of a volcanic edifice. The volcanic units are transported in a water unsaturated (but not necessarily exclusively dry) gravity-driven mass at speeds of 20–100 m s^{-1}, referred to as a volcanic debris avalanche [Bernard et al. 2021]. The associated accumulated debris is a volcanic debris avalanche deposit (VDAD).

Historically, large volcanic island landslide events have only been observed in volcanic arc settings; however, evidence indicates that such events are commonplace in the geological history of oceanic intraplate volcanoes [Watt et al. 2021]. This evidence includes collapse scars and/or their seafloor deposits [Siebert 1984; Masson et al. 2002; Oehler et al. 2007]. Bathymetric data indicate that volcanic landslides are frequent and repetitive processes in the construction and destruction cycle of volcanic islands, occurring every 10s to 100s of thousands of years [McGuire 1996; Capra et al. 2002; Zernack 2021]. Understanding the scale and triggers of past volcanic landslides in isolated oceanic intraplate settings is important because recent events have demonstrated the significant regional and global climatic and human impacts of unexpected volcanic events at relatively isolated, understudied volcanoes in oceanic settings e.g. Hunga Volcano 2021–2022 [Lynett et al. 2022; Carter et al. 2023].

Extensive submarine volcanic debris avalanche deposits have been mapped around 40 oceanic intraplate volcanoes including the Canary Islands [Krastel et al. 2001], Réunion Island [Oehler et al. 2007], and the Hawaiian Islands [Moore et al. 1994; McMurtry et al. 2004]. More recently, 182 landslides have been compiled in a worldwide database of volcanic island landslides across the Atlantic, Pacific, and Indian oceans [Blahůt et al. 2019; Rowberry et al. 2023]. Regional and global compilations such as these represent a substantial effort and enable a broad view of the spatial distribution, scale, and impact of volcanic island landslides. Yet due to limited data availability, particularly in the submarine environment, the full spatial extent and the timing of many volcanic island landslides remains absent from such compilations.

* sally.watson@niwa.co.nz

Submitted: 2024-03-22 | Accepted: 2024-09-24 | Published: 2025-01-27

Editor: J. Farquharson | Typesetter: A. G. Ryan

Here we present the first submarine geomorphological, geochemical, and geochronological evidence for a volcanic landslide at sub-Antarctic Heard Island, southern Indian Ocean, using multibeam bathymetry data and geological samples collected during the IN2016_V01 voyage of Australia's Marine National Facility RV *Investigator*. We determine the extent, volume, and timing of the volcanic landslide and evaluate potential triggers. Lastly, we present future implications for landslides at Heard Island.

2 Volcanism on Heard Island

Heard Island is an active, largely unmonitored intraplate volcanic island, mostly covered by glaciers, located on the Kerguelen Plateau in the southern Indian Ocean (Figure 1A–C). The Kerguelen Plateau is a mainly submarine, large igneous province produced by voluminous basaltic eruptions attributed to the activity of Kerguelen hotspot over the last 130 Myr (Figure 1B) [Coffin et al. 2002]. Volcanism at Heard Island is understood to be the current subaerial expression of the active Kerguelen hotspot [Barling et al. 1994]; the most recent eruption occurring in April 2024. Heard Island's two main volcanic centres, Laurens Peninsula and Big Ben (Figure 1C), have been constructed on a basement of Oligocene Laurens Peninsula Limestones and Pliocene Drygalski Formation lavas and volcaniclastic sediments [Stephenson 1964; Barling et al. 1994; Truswell et al. 2005; Duncan et al. 2016]. The Drygalski Formation is a succession of submarine basaltic lavas and associated clastic units form a ~300 m-thick platform now exposed above sea level [Barling et al. 1994; Fox et al. 2021]. Lavas from the two volcanic centres are known collectively as the Newer Lavas and are divided into the Laurens Peninsula Series (LPS) and the Big Ben Series (BBS) based on compositional differences between the two volcanic centres [Barling et al. 1994]. The Laurens Peninsula volcanic complex comprises basanitic lavas and trachytic domes [Barling 1994]. LPS lavas have distinctly lower Sr ($^{87}Sr/^{86}Sr$ 0.7047–0.7059), and higher Nd (εNd +0.6–+2.0) and Pb isotope ratios ($^{206}Pb/^{204}Pb$ 18.53–18.83) in comparison to the BBS lavas ($^{87}Sr/^{86}Sr$ 0.7052–0.7079, $^{206}Pb/^{204}Pb$ 17.790–18.211, and εNd −0.2 to −4.6) [Barling et al. 1994]. Big Ben, a stratovolcano complex, is dominated by basanite, alkali basalt, and trachybasalt [Barling et al. 1994]. The known volcanic history of the Newer Lavas, particularly the BBS, is fragmentary due to extensive ice cover and paucity of data [Duncan et al. 2016; Fox et al. 2021]. The youngest age for the underlying Drygalski Formation is 720 ± 78 ka for a sample collected on Laurens Peninsula, providing an estimate for the earliest onset of Newer Lavas volcanism of ca. 798 ka [Duncan et al. 2016]. The $^{40}Ar/^{39}Ar$ ages of the LPS are 387 ± 31 ka and 76.6 ± 5.5 ka to 5.1 ± 3.5 ka, and BBS lavas 180 ± 18 ka, and 53.3 ± 2.3 ka to 7 ± 7 ka [Duncan et al. 2016; Fox et al. 2021]. Young (1.9 ± 3.8 to 13.3 ± 4.1 ka) basaltic pyroclastic cones are located around the coast of Heard Island [Fox et al. 2021]. Historical volcanic activity has been focussed at Mawson Peak, a volcanic cone located at the summit of Big Ben (2813 m) [Quilty and Wheller 2000; Fox et al. 2021]. The only sample collected from a historical lava (1985 eruption) is basanite in composition [Barling et al. 1994].

3 Heard Island morphology and the volcanic landslide scar

Big Ben's morphology is characterised by the presence of ridges radiating from the central summit crater except on the southern flank [Quilty and Wheller 2000; Fox et al. 2021].The ridges comprise eroded lavas and pyroclastic deposits on the western flanks; the remainder have not been examined and could comprise similar lithologies or be exhumed dykes or ice-marginal lavas [Stephenson 1964; Fox et al. 2021]. Extensive glaciers occupy the space between the ridges. The summit crater is an open horseshoe shape and Mawson Peak has been constructed overlapping the northwestern rim of the crater (Figure 1C) [Stephenson et al. 2005]. The absence of ridges on the southern flank together with the open horseshoe shape of the summit crater have been interpreted to be the product of a sector collapse towards the south of Big Ben prior to the formation of Mawson Peak [Quilty and Wheller 2000; Stephenson et al. 2005]. Fox et al. [2021] suggested that the basaltic lavas at Cape Arkona could be remnant lavas not removed during the collapse. Their $^{40}Ar/^{39}Ar$ age, 23 ± 16 ka [Duncan et al. 2016] provides a potential maximum age for the volcanic landslide.

Glaciers and the recent retreat of glaciers on Heard Island have modified and carved the onshore landscape of Heard Island, creating glacial landforms including moraines, cirques, glacial valleys and ridges, and meltwater lakes, as well as glacial till deposits [Kiernan and McConnell 1999]. Today, Heard Island (~368 km^2) has 12 major glaciers, some extending from the summit to sea level [Kiernan and McConnell 1999; Ruddell 2006; Hodgson et al. 2014]. Evidence for the growth and retreat of glaciers in the vicinity of Heard Island has relied on historical records and observations, monitoring of glacial extent onshore [Kiernan and McConnell 1999; Kiernan and McConnell 2002; Thost and Truffer 2008], remote sensing [Thost and Truffer 2008; Cogley et al. 2014], and 100 m resolution bathymetric compilations [Balco 2007; Beaman and O'Brien 2011; Hodgson et al. 2014]. Geomorphological evidence suggests past extensive glaciation of Heard and McDonald Islands and an ice cap on a surrounding portion of the Central Kerguelen Plateau, likely dating back to the Last Glacial Maximum (ca. 26.5–19 ka) with an extent of 9585 km^2 (Figure 1C) [Balco 2007; Hodgson et al. 2014].

4 Methods and Samples

4.1 Bathymetry

In 2016, RV *Investigator* acquired the first multibeam bathymetry data around Heard Island, mapping 20 % of the seafloor within the territorial seas of the Heard Island and McDonald Islands Marine Reserve. Multibeam data were collected using a hull-mounted Kongsberg EM710 shallow water (<1000 m) multibeam echosounder, with a frequency range of 70–100 kHz (0.5 × 1°). Multibeam bathymetry data were processed on board using Caris HIPS and SIPS 8.1 and gridded at 5 m resolution.

Seafloor backscatter data were processed using the QPS `Fledermaus Geocoder Toolbox` (`FMGT`) and gridded at 15 m resolution. Swath lines that contained extensive artefacts due

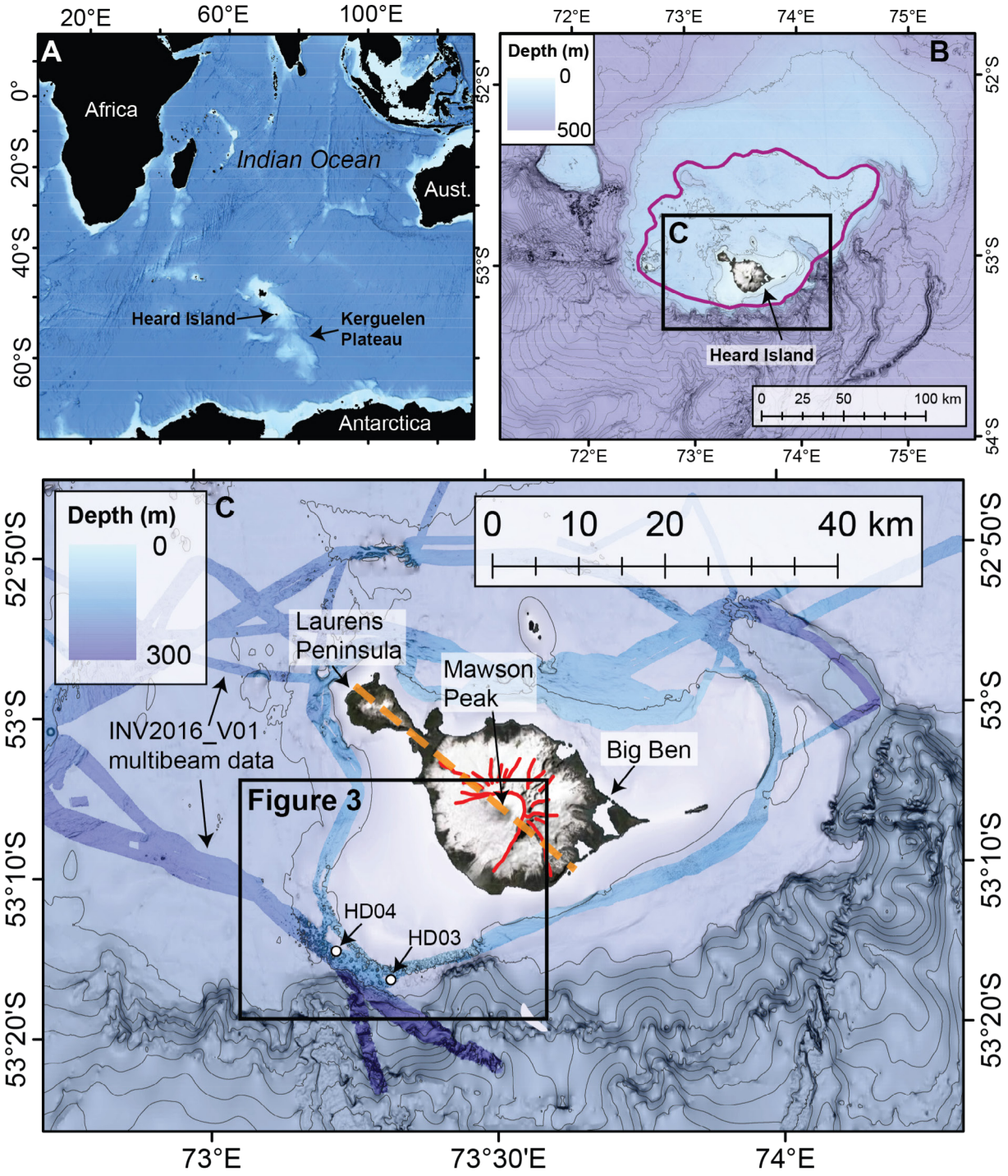

Figure 1: Heard Island location. [A] The Indian Ocean showing the location of the Kerguelen Plateau and Heard and McDonald Islands. Bathymetry data is [GEBCO 2023], Mercator projection. [B] Background bathymetry data is [Beaman 2023] 100 m resolution bathymetry grid of Heard and McDonald Islands, with 100 m contours. WGS84, UTM43S. Black box shows location of Figure 1C. Purple line shows estimated location of LGM glacial extent from Balco [2007] and Hodgson et al. [2014]. [C] Bathymetry and topography map of Heard Island and surrounds. Background bathymetry data is from [Beaman 2023] 100 m resolution bathymetry grid of Heard and McDonald Islands, with 100 m contours. Multibeam data collected on INV2016_V01 [Coffin et al. 2023] is overlain at 5 m resolution. Red lines highlight radial ridges and the margins of the southwest facing horseshoe-shaped crater [Fox et al. 2021]. Black box shows the location of Figure 3 WGS84, UTM43S. White dots with black border are dredge locations and names (HD03 and HD04). Orange dashed line indicates alignment of volcanic cones and vents, faults, and the broader geographic alignment of Big Ben and Laurens Peninsula suspected to be structure-related [Fox et al. 2021].

to adverse sea state were removed from the final seafloor backscatter mosaic. Multibeam data were interpreted using ArcGIS 10.8.2. Geomorphological analyses including the rugosity derivative were performed using the Benthic Terrain Modeler (BTM) toolbox 3.0 [Walbridge et al. 2018]. Rugosity, also known as Terrain Ruggedness, measures the small-scale variation, complexity, and roughness. The rugosity tool provides a raster that measure the surface area of a neighbourhood compared to the planar area as a ratio (where values nearer to zero have less terrain variation than values closer to one.

4.2 Samples

Two hummocks within the suspected VDAD south of Big Ben were dredged during IN2016_V01, HD03 and HD04 (Figure 1, Table 1). Basaltic lavas, basaltic breccias, tuffaceous sandstones, and pumice were recovered (Supplementary Material 1 Table S1, Figure S1). Samples have a broad size range (diameter 2–60 cm) and are angular to rounded. Fresh, non-vesicular to moderately vesicular olivine-clinopyroxene±plagioclase phyric basaltic lavas are the dominant rock types for both dredges (Figure 2A, 2B, Supplementary Material 1 Table S1A–E). Reddened, moderately to highly vesicular basaltic lavas comprise <5 % of the rocks recovered (Supplementary Material 1 Figure S1F). Basaltic breccias comprise pebble- to gravel-sized polymictic basaltic clasts in a matrix of glass, Fe-Ti-oxide, and olivine fragments (Figure 2C,D, (Supplementary Material 1 Figure S1G and H). Brown, tuffaceous sandstone interbedded with siltstone was recovered from dredge HD03 only and is composed of smectite, Fe-Ti oxides, basaltic lithic clasts, and devitrified glass. Rounded grey-green pumice was recovered from dredge HD03 (Supplementary Material 1 Figure S1I). Five representative, fresh lavas were selected for further analysis (Table 1). The pumice was not investigated further because it is macroscopically resembles phonolitic pumice that arrived at Heard Island via a pumice raft following the 1997 eruption of McDonald Island [Stephenson et al. 2006], 43 km east of Heard Island.

4.3 Whole rock geochemistry

4.3.1 *Whole rock major and minor element analysis*

Whole rock major elements for five representative coherent lava samples (Table 1) were obtained via XRF with a PANalytical Axios Advanced X-Ray Spectrometer at the Centre for Ore Deposits and Earth Sciences (CODES), University of Tasmania (Australia). Whole rock minor elements were obtained via solution-ICP-MS technique using an Agilent®-7700x instrument at the CODES, University of Tasmania, Australia. Detailed methods are provided in the Supplementary Material 1 and Supplementary Material 2.

4.3.2 *Sr-Nd-Pb-Hf isotopes*

Radiogenic isotope data for two selected samples (Table 1) were acquired at the University of Melbourne [Maas et al. 2005]. Splits of agate-milled powders (100–140 mg) were leached with 6M HCl (100 °C, 60 min) and digested at high pressure (HF, 160 °C, 48 hrs; HCl, 160 °C, 12 hrs). Pb was extracted on small columns of AG1-X8 (100–200) anion exchange, using the HBr-HCl technique. Hf, Nd, and Sr were extracted from the HBr eluate of the Pb column, using Eichrom LN-, TRU/LN, and Sr resin, respectively [Münker et al. 2001; Pin et al. 2014]. Total analytical blanks (~50 pg for Pb and Hf; ≤100 pg for Nd and Sr) are negligible compared to the amounts of Pb, Hf, Nd, and Sr processed.

All isotopic analyses were carried out on a Nu Plasma multi-collector ICP-MS with sample introduction via a low-uptake Glass Expansion PFA nebuliser and a CETAC Aridus desolvator. Sensitivity in this set-up is in the range of 130–150 V/ppm Sr, Nd, Pb, or Hf. Instrumental mass bias in Nd, Sr, and Hf analyses was corrected by normalizing to $^{146}Nd/^{144}Nd = 0.7219$, $^{86}Sr/^{88}Sr = 0.1194$, and $^{179}Hf/^{177}Hf = 0.7325$, respectively, using the exponential law. $^{143}Nd/^{144}Nd$, $^{87}Sr/^{86}Sr$, and $^{176}Hf/^{177}Hf$ are reported relative to La Jolla Nd = 0.511860, SRM987 = 0.710230, and JMC475 = 0.282160. Results for USGS rock and other standards are consistent with TIMS and MC-ICP-MS reference values. Typical in-run precisions (2σ) are ± 0.000010 (Nd), ± 0.000016 (Sr), and ± 0.000008 (Hf). External (2σ) precisions are ± 0.000020, ± 0.000040, and ± 0.000015, respectively. Mass bias for Pb was corrected using the thallium-doping technique [Woodhead 2002]. This produces data with an external precision (2σ) of ± 0.04–0.06 % for $^{206}Pb/^{204}Pb$ and $^{207}Pb/^{204}Pb$, and 0.07–0.09 % for $^{208}Pb/^{204}Pb$.

4.4 $^{40}Ar/^{39}Ar$ geochronology

We selected one sample from each of the dredge sites (Table 1) for $^{40}Ar/^{39}Ar$ age determinations. We obtained high-purity basalt groundmass concentrates (>99 % purity) by crushing and sieving (150–250 µm size), then removing phenocryst phases (ol, cpx, pl) by Frantz magnetic separator and hand-picking under binocular microscope. We treated groundmass separates in a series of acid leaching steps: 1N and 6N HCl, 1N and 3N HNO_3, followed by ultrasonic washing in triple distilled water (3X) to remove any remaining fine particles.

We encapsulated between 40 and 20 mg of high purity groundmass in aluminium foil and interspersed packets with a standard of known age (FCT-NM-Fish Canyon Tuff sanidine, 28.201±0.023 Ma, 1σ [Kuiper et al. 2008]) and vacuum sealed the samples with standards in quartz vials. The samples were irradiated for 30 minutes at 1 MW power (Irradiation 16-OSU-05) in the TRIGA (CLICIT-position) nuclear reactor at Oregon State University.

We produced $^{40}Ar/^{39}Ar$ age data by incremental heating experiments using an ARGUS-VI mass spectrometer with 25W CO_2 laser and associated high vacuum system (see instrument description in Supplementary Material 3). Sample heating occurred in steps (by increasing laser power), following an initial surface degassing, up to fusion. The heating schedule, based on experience with basaltic compositions and sample weights, produced 27 gas release steps, which is sufficient to resolve reliable age information from potential alteration (Ar-loss) and experimental artifacts (Ar-recoil) without sacrificing step age precision. We calculated ages using the corrected Steiger and Jäger [1977] decay constant of $5.530 \pm 0.097 \times 10^{-10}$ yr^{-1} (2σ) as reported by Min et al. [2000] and the Lee et al. [2006] value for trapped atmospheric

8(1): 31–50. https://doi.org/10.30909/vol.08.01.3150

Table 1: Location and petrographic description of representative lava samples selected for analysis from dredges HD03 and HD04.

Sample number	Field sample number	Dredge number	Latitude degrees	Longitude degrees	Depth (m)	Petrographic description	Composition	Whole rock geochem.	$^{40}Ar/^{39}Ar$ geochron.	Sr-Nd-Pb-Hf isotopes
KP-03-09A	HD03-009	HD03	−53.28	73.32	−162	ol+cpx+plg-phenocrysts in ground mass of glass and plg microlites	alkalic basalt	X		
KP-03-10	HD03-010	HD03	−53.28	73.32	−162	ol+cpx+plg-phenocrysts in glassy ground mass	trachybasalt	X	X	
KP-03-17B	HD03-017B	HD03	−53.28	73.32	−162	ol+cpx-phenocrysts in ground mass of glass and pyx microlites	basanite	X		X
KP-04-06A	HD04-006A	HD04	−53.25	73.23	−132	cpx+ol-phenocrysts in a glassy ground mass	trachybasalt	X	X	X
KP-04-09	HD04-009	HD04	−53.25	73.23	−132	ol+cpx+plg-phenocrysts in a glassy ground mass	trachybasalt	X		

Table 2: $^{40}Ar/^{39}Ar$ age determinations for sea knolls near McDonald Islands and Heard Island. Analytical results are supplied in the Supplementary Material 4-6.

Sample number	Plateau age ± 2σ	Total ^{39}Ar released (%)	MSWD[a]	n[b]	Normal isochron age ± 2σ	$^{40}Ar/^{36}Ar$ ± 2σ intercept	MSWD	Inverse isochron age ± 2σ	$^{40}Ar/^{36}Ar$ ± 2σ intercept	MSWD	J-value (flux monitor)
KP-03-10	38.1 ± 4.1 ka	100	0.54	27	35.1 ± 8.8 ka	299.16 ± 1.55	0.56	35.2 ± 7.9 ka	299.16 ± 1.55	0.55	0.0001323
KP-04-06A	18.0 ± 1.4 ka	63.52	0.89	7	13.7 ± 7.1 ka	303.73 ± 8.41	0.78	13.7 ± 6.3 ka	303.77 ± 8.42	0.78	0.0001311

[a] MSWD is an F-statistic that compares the variance within step ages with the variance about the plateau age.
[b] Number of analyses included in the isochron.

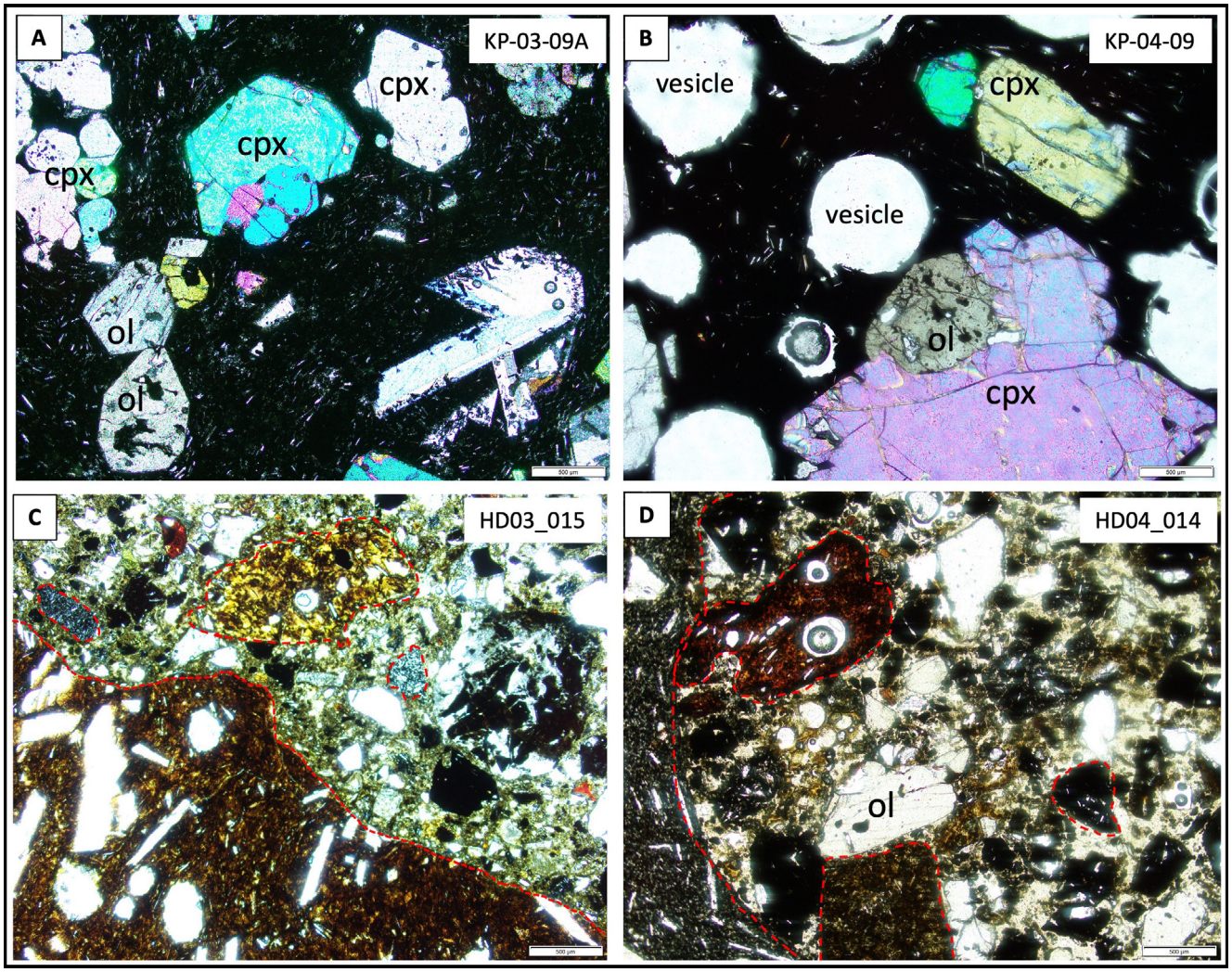

Figure 2: Photomicrographs of representative samples from dredges HD03 and HD04. [A] KP-03-09A (HD03), alkali basalt under XPL. [B] KP-04-09 (HD04), trachybasalt under XPL. [C] HD03_015, basaltic breccia under XPL. [D] HD04_014, basaltic breccia under PPL. Red dashed lines outline the boundaries of selected basaltic clasts. For dredge locations see Figure 3A.

$^{40}Ar/^{36}Ar$ (298.56 ± 0.31). For all other constants used in the age calculations we refer to Table 2 in Koppers et al. [2003].

The term "plateau age" refers to the weighted mean age [Taylor 1997] of multiple, contiguous temperature steps with apparent ages that are indistinguishable at the 95 % confidence interval and represent 50 % or more of the total ^{39}Ar released [Fleck et al. 1977]. We used isochron analyses [York 1968] to assess if non-atmospheric argon components were trapped in either sample, and to confirm the plateau ages. A total gas age (Total Fusion), similar to a conventional K-Ar age, was calculated by summing all gas fractions for each sample. All calculations used the `ArArCALC` software [Koppers 2002] v2.5.2*. Summaries of experimental data are provided in the Supplementary Material 4. Full data tables, including step % laser power, age, % radiogenic ^{40}Ar, % $^{39}Ar_K$, and K/Ca, normal and inverse isochron data, regression statistics, and procedure blanks are provided in Supplementary Material 5 and Supplementary Material 6.

*Available from the `http://earthref.org/ArArCALC/` website

5 Results

5.1 Bathymetry and seafloor backscatter

The Heard Island landslide scar is delineated by a SW facing headscarp and adjoining lateral scarps (Figure 3A). Downslope of the headscarp, ~15 km from the modern coastline, multibeam bathymetry (including bathymetric derivatives) and seafloor backscatter data (Figure 3A–3C) reveals the seafloor to be highly irregular with abundant blocky debris (Figure 3A). The seabed is characterised by relatively high intensity backscatter return compared to the background low signal return (Figure 3B). The high backscatter and high rugosity region broadly forms a lobate shape (Figure 3C), laterally expanding from the onshore lateral scarps ~11 km apart to an offshore width of at least 28.6 km (Figure 3C). The mapped boundaries of the high-rugosity, high backscatter lobe vary, with the estimated broadest limits shown in Figure 3A–3C. The eastern limits of the lobe are characterised by a sharp contrast between high-rugosity and high backscatter seabed, compared to the relatively smooth, low backscatter seabed

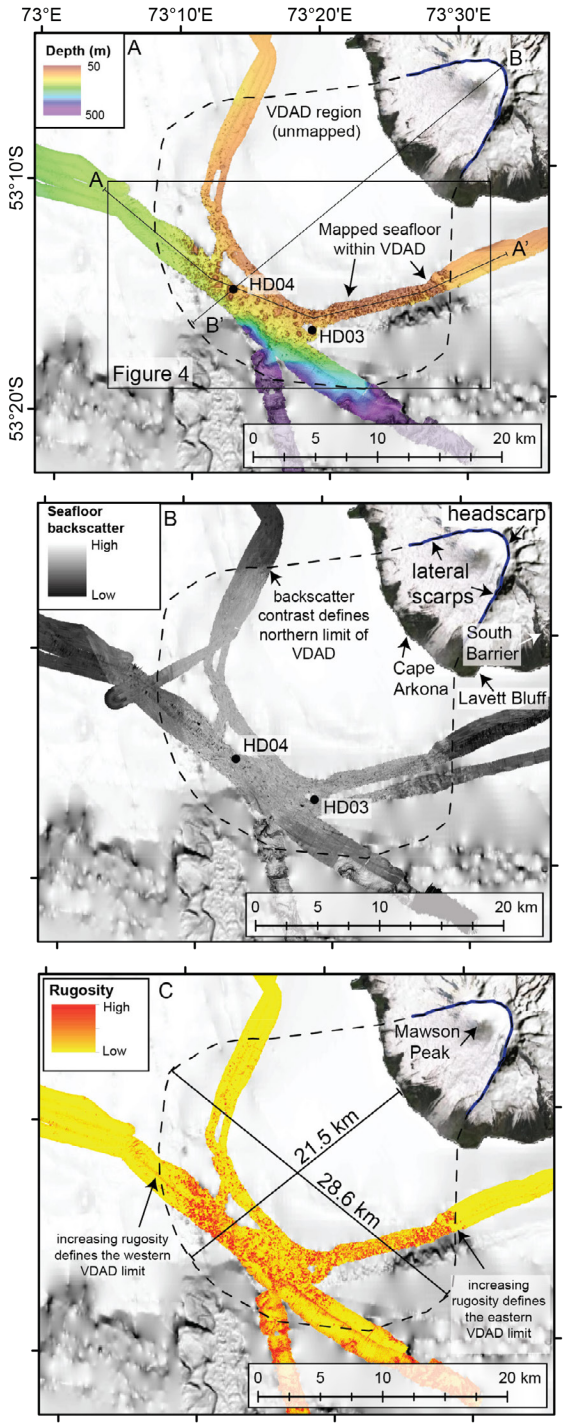

Figure 3: The Heard Island volcanic debris avalanche deposit (VDAD). Multibeam data (5 m resolution) collected on INV2016_V01 [Coffin et al. 2023] is overlain on grey-scale bathymetry data (100 m resolution) from Beaman [2023]. [A] Multibeam bathymetry. [B] Seafloor backscatter. Black circles on [A] and [B] show dredge locations. [C] Seabed rugosity on the SW margin of Heard Island. Dashed black line denotes the observable limits of the VDAD as indicated by variable blocky debris, high seafloor backscatter and increased rugosity, compared to adjacent seafloor. The location of Figure 4 and the profiles presented in Figure 4B, 4C are shown in [A].

to the east (Figure 4A). The northern limit shows a distinctive change from low to high intensity backscatter, but with fewer blocky deposits and more subdued change in morphology (Figure 3B). The western and southern limits are characterised by a gradual decrease in blocky, rugose seabed with distance from Big Ben (Figure 4A). Individual blocks are up to 80 m taller than the surrounding seabed and span several hundred metres across (Figure 4B). Using these data, we estimate the spatial extent of the high-rugosity, high backscatter lobe ~ 21.5 km long and ~28.6 km wide, with a total estimated offshore area of 467 km^2 (Figure 3A–3D). The average slope from the onshore headscarp to the estimated proposed submarine limit is 4.5°; the average slope onshore is 12.6° and offshore is <1° (Figure 4C).

5.2 Whole rock compositions

Whole rock loss on ignition values (LOI < 0.99 wt%, Supplementary Material 2 Table S2) indicate the samples are fresh, consistent with the absence of petrographic evidence for seafloor weathering or alteration. Major element compositions reveal the volcanic rocks from dredge HD03 are trachybasalts and those from dredge HD04 are alkalic basalt, trachybasalt, and basanite (Figure 5A, Supplementary Material 2 Table S2). For the trachybasalts and alkalic basalt, SiO_2 and TiO_2 have relatively low variability with increasing MgO (Figure 5B, 5C). Incompatible trace element ratios, e.g. Rb/Ba, Ba/Nb, and La/Nb (Figure 5D–5F, Supplementary Material 2 Table S2) show little variation with MgO for all dredged samples. The new whole rock composition data plot mainly with the basanite and the basalt-trachybasalt groups from the BBS and do not overlap with the LPS lavas (Figure 5).

The dredged samples have LREE-enriched REE patterns parallel to and plotting within the range of values displayed by BBS lavas (Supplementary Material 2 Figure S2A). On a primitive mantle-normalised diagram (Supplementary Material 2 Figure S2B), the dredged samples show the distinctive enrichment of Ba relative to Nb which is characteristic of the BBS lavas [Barling et al. 1994].

Sr, Nd, and Pb isotope ratios of the new samples, $^{87}Sr/^{86}Sr$ 0.7051 and 0.7059, $^{206}Pb/^{204}Pb$ 18.17 and 18.09, and εNd +0.5 and −1.5 (Supplementary Material 2 Table S2) fall within the ranges previously reported for the Heard Island Newer Lavas [Barling et al. 1994] (Figure 6). When plotted with these published data, the new isotopic ratios plot with the BBS data rather than the LPS data (Figure 6). Hf isotopic ratios for the dredged samples are $^{176}Hf/^{177}Hf$ 0.2828 and 0.2828 (εHf 2.2278, −0.14145) (Supplementary Material 2 Table S2), consistent with values expected for ocean island basalts. No Hf isotopic ratios have been published for Heard Island lavas for further comparison.

5.3 $^{40}Ar/^{39}Ar$ geochronology

We report two $^{40}Ar/^{39}Ar$ age determinations (Figure 7) and summarise analytical results in Table 2 (and see Supplementary Material 4–Supplementary Material 6). Sample KP-03-10, an olivine-clinopyroxene-plagioclase-phyric trachybasalt from dredge HD03, produced a plateau age of 38.1 ± 4.1 ka (27 step plateau, 100 % of ^{39}Ar released) (Table 2, Figure 7A).

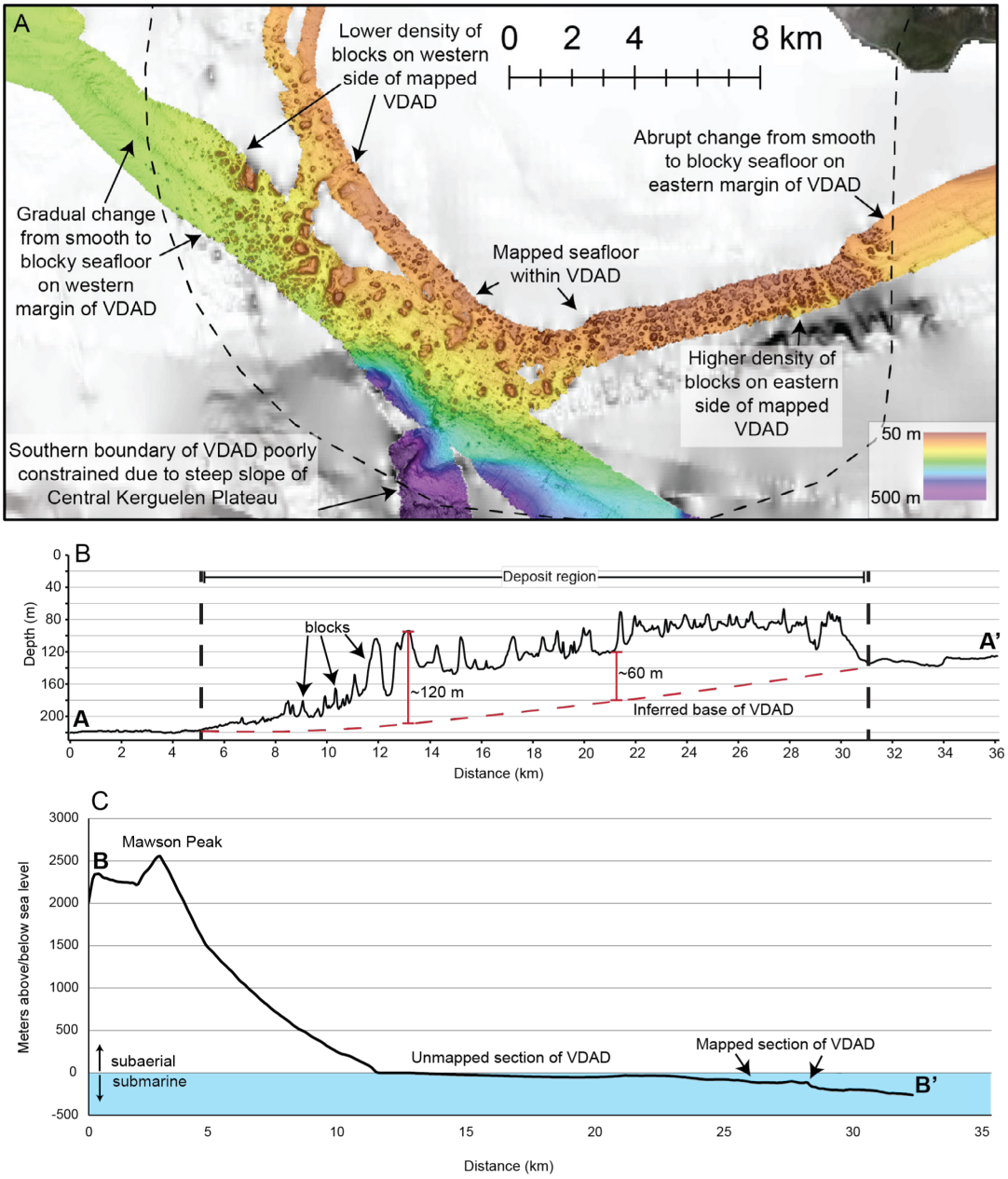

Figure 4: Details of the VDAD southwest of Heard Island. [A] Inset of the mapped region within VDAD showing the relative change in block density from east to west, particularly on the boundaries of the VDAD. Multibeam data (5 m resolution) collected on INV2016_V01 [Coffin et al. 2023] is overlain on grey-scale bathymetry data (100 m resolution) from Beaman [2023]. [B] Profile A–A' across the debris deposit shows the difference between the flat and smooth seabed, and the chaotic, debris deposit, downslope from the landslide headscarp. The inferred base of VDAD is estimated with red dashed line [C]. Profile B–B' onshore Heard Island to offshore showing the vertical change from the source area (onshore Heard Island) to the deposit area. The region mapped with multibeam echosounders is labelled, the remaining profile has been obtained from topographic and bathymetric data from Beaman [2023]. The location of both Profile A–A' and B–B' is presented in Figure 3A. For the location of this image, see Figure 3A.

The normal isochron ($^{40}Ar/^{36}Ar$ vs. $^{39}Ar/^{36}Ar$) and inverse isochron ($^{36}Ar/^{40}Ar$ vs. $^{39}Ar/^{40}Ar$) ages, using the same steps, confirm the plateau age and yield $^{40}Ar/^{36}Ar$ intercepts that are within analytical error of atmospheric composition (298.56). The mean square of weighted deviations (MSWD) for plateau and isochrons are <1, indicating that the ages are statistically reliable [Schaen et al. 2021]. Sample KP-04-06A a clinopyroxene-olivine-phyric trachybasalt from dredge HD04 yielded a plateau age of 18.0 ± 1.4 ka (7 step plateau, 64 % of ^{39}Ar released) (Table 2, Figure 7B). Isochron ages and intercepts confirm the plateau age, and the MSWDs are appropriately low. The lavas from the dredged hummocks returned

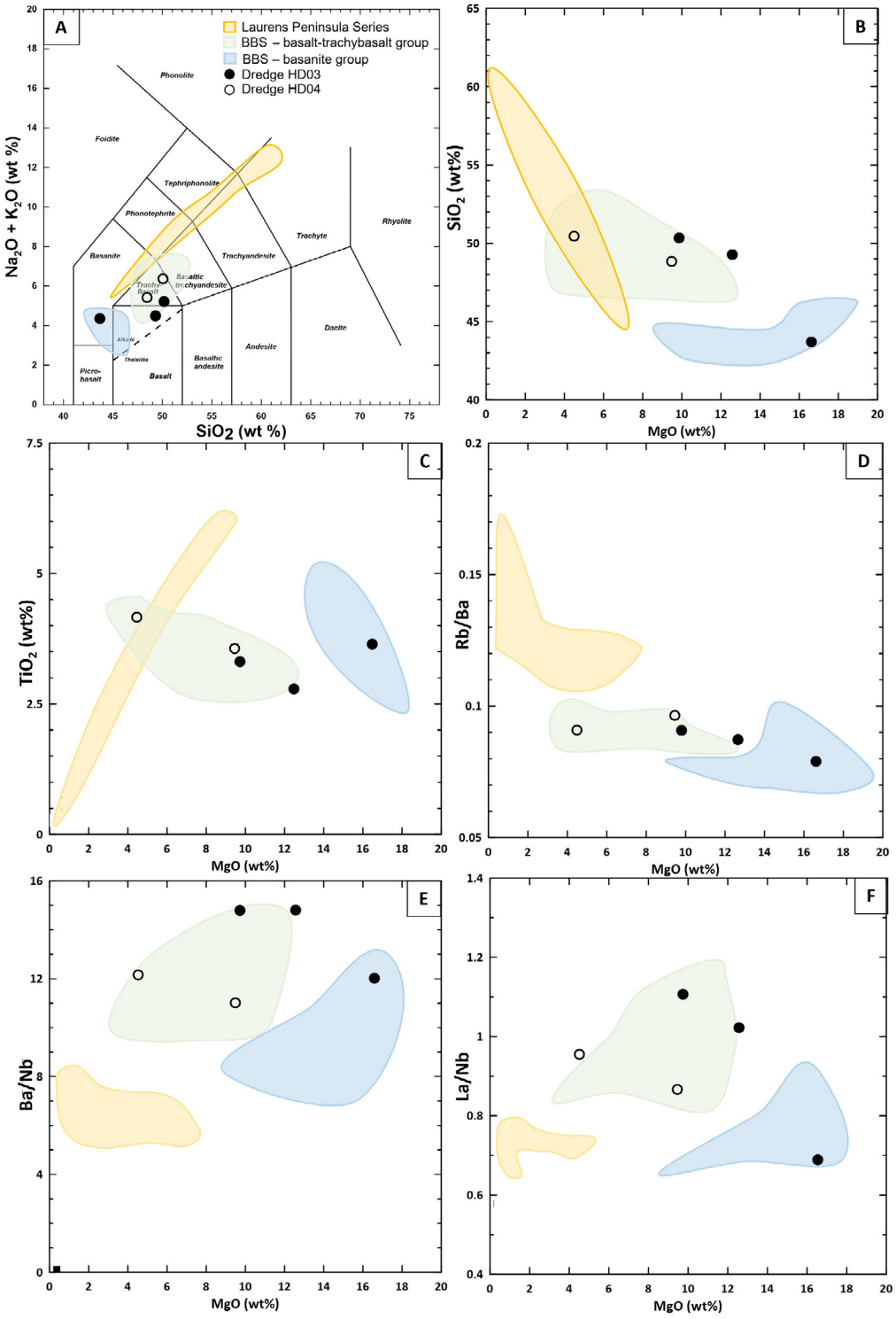

Figure 5: Whole rock geochemistry samples from dredges HD03 and HD04 (this study) plotted with published data for Big Ben Series (*BBS) and Laurens Peninsula Series lavas from Heard Island [Barling et al. 1994]. [A] Total alkali–silica classification (solid lines) [Le Maitre et al. 2002] and empirical alkalic–tholeiitic boundary line (dashed line) [MacDonald and Katsura 1964]. [B-D] Selected major elements (wt%) and [E-F] selected trace element ratios versus MgO (wt%).

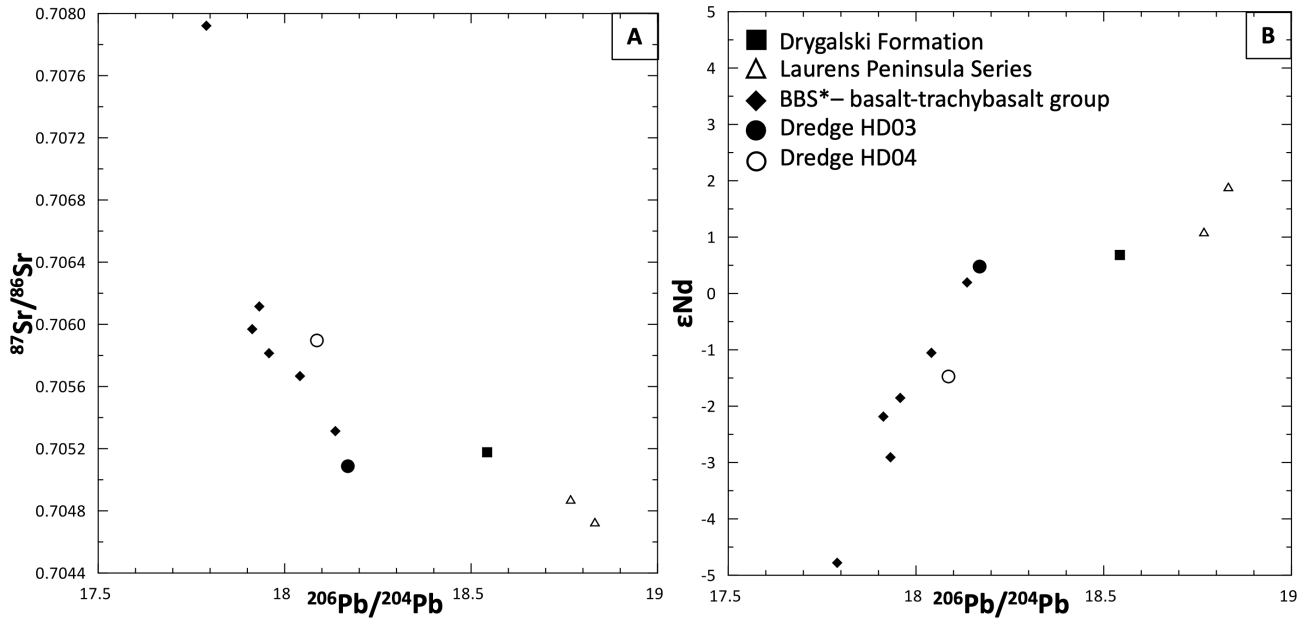

Figure 6: Sr, Pb and Nd isotopic compositions for selected samples from dredges HD03 and HD04 (this study) and published Heard Island lava samples [Barling et al. 1994]. [A] $^{206}Pb/^{204}Pb$ and $^{87}Sr/^{86}Sr$. [B] $^{206}Pb/^{204}Pb$ and εNd *Big Ben Series.

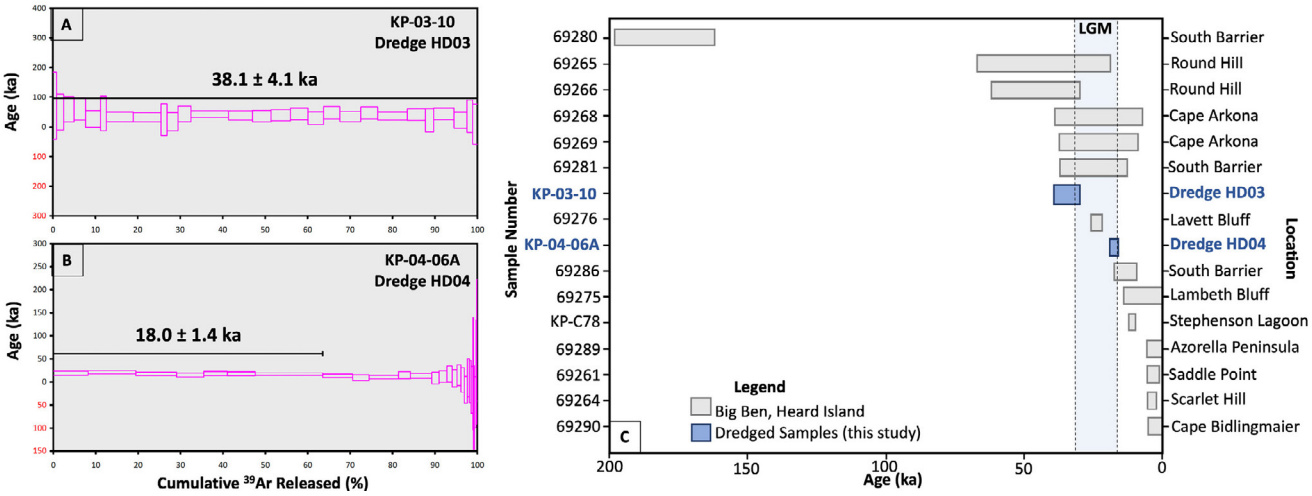

Figure 7: $^{40}Ar/^{39}Ar$ geochronology results. Errors on plateau (>50 % ^{39}Ar released) age are quoted at 2σ and do not include systematic errors (i.e. uncertainties on the age of the monitor and on the decay constant). [A] Sample KP-03-10 is a trachybasalt, 27 step plateau, 100 % ^{39}Ar released, MSWD 0.54. MSWD is an F-statistic that compares the variance within step ages with the variance about the plateau age. [B] Sample KP-04-06A is a trachybasalt, 7 step plateau, 63.52 % ^{39}Ar released, MSWD 0.89. [C] Ages of dredged samples plotted with published $^{40}Ar/^{39}Ar$ ages for Big Ben lavas [Duncan et al. 2016; Fox et al. 2021]. Dredged samples are similar in age to lavas from the southern slopes of Big Ben, Heard Island e.g. Cape Arkona, South Barrier, Lavett Bluff (see Figure 3B for locations), and 6 km to the east at Lambeth Bluff.

ages that overlap with dated BBS lavas (Figure 7C) and are similar in age to lavas from the southern slopes of Big Ben, Heard Island e.g. Cape Arkona, South Barrier, Lavett Bluff (see Figure 3B for locations).

6 Discussion

6.1 Evidence for volcanic landslide at Heard Island

We interpret one or more volcanic landslide(s) on the southern sector of Big Ben on the basis of the following evidence: (1) the presence of a landslide scar onshore Big Ben [Quilty and Wheller 2000; Fox et al. 2021], (2) morphology of the seafloor offshore southwest Heard Island is consistent with a landslide deposit [Bernard et al. 2021], (3) the spatial relationship between the landslide scar onshore Big Ben and the landslide deposit [e.g. Krastel et al. 2001], and (4) lithologies and compositions of rocks sampled from the landslide deposit are consistent with onshore *in situ* lithologies of Big Ben.

The Heard Island volcanic landslide had been inferred by onshore morphological evidence [Stephenson et al. 2005;

Quilty 2007]. This study represents the first attempt to identify the offshore spatial extent of the associated debris using multibeam bathymetry and backscatter data show a region of high-backscatter and rugosity occupies the shallow submarine shelf to the southwest of Heard Island, extending ~32 km from the headscarp, and ~21.5 km from the present coastline (Figure 3A, Figure 4C). The northern, eastern and western boundaries of this region (Figure 3A–3C, Figure 4A) clearly indicate changes in seafloor morphology and the nature of the seabed, as inferred by contrasting seafloor backscatter returns. We interpret this region to be debris associated with the onshore landslide scar and refer to this region hereafter as a VDAD.

The seafloor within the VDAD is characterised by relatively undulating relief and slope (up to 30° within the VDAD, compared to <4° across adjacent seafloor), higher intensity seafloor backscatter, and increased rugosity, compared to adjacent seafloor to the north, northwest, and east, (Figure 3A–3C, Figure 4A, 4B). The seafloor mapped within the VDAD is variable, shown by the relatively high density of blocks in the eastern portion, compared to the western and northern portions (Figure 4A). This could indicate multiple lobes, associated with one or more events. However, due to the relatively limited surveyed region used to characterise this VDAD (only ~20 % of estimated VDAD area was mapped), it is difficult to make robust observations about the character of the entire VDAD. With the current dataset, it is not possible to pursue a detailed assessment of the deposit structure, delineation of distinct lobes, number of events, or landslide block orientation, nor to conclude whether this represents one, or several landslide event(s).

The high intensity backscatter signature indicates the VDAD is characterised by a distinct, likely harder and/or coarser sediment substrate. The broadscale lobate morphology of the deposit, along with the onshore scar geometry is consistent with a southwest failure direction. The debris comprises hummocky, undulating terrain, inferred to be intact fragments of the volcano flank that have been transported downslope during one or more gravitational events. VDAD blocks are up to 80 m in height, in some cases several hundred metres across, and lie ~15 km from the modern coastline (Figure 3D), although there are likely many more beyond the surveyed region. The preservation of such large blocks suggests that the landslide event(s) was/were sufficiently energetic to transport these blocks several kilometres over submarine slopes ≤ 4° (Figure 4C). Furthermore, the presence of such large landslide blocks in other volcanic island landslides has been used to indicate minimal block interaction during the failure event (e.g. Anak Krakatau [Hunt et al. 2021]) and relatively rapid emplacement (e.g. South Kona, Hawai'i [Moore et al. 1995]).

Lithologies dredged from the debris blocks within the VDAD include glassy basaltic volcaniclastic breccias and sandstones (Supplementary Material 1 Figure S1) texturally similar to those previously described for the Drygalski Formation [Lambeth 1952; Stephenson 1964; Fox et al. 2021]. The geochemical compositions and mineralogy of the lavas dredged from the VDAD, including isotopic compositions, are consistent with the published compositions of BBS lavas (Figure 5, Figure 6) [Barling et al. 1994]. The presence of a mixture of Drygalski Formation-like volcaniclastic rocks and BBS-like lavas in a poorly sorted, hummocky submarine deposit adjacent to the coast of the Big Ben part of Heard Island is interpreted to indicate that they have been transported in a gravity driven mass flow (debris avalanche) from onshore Big Ben [Siebert 1984; Bell et al. 2013; Dufresne et al. 2021; Watt et al. 2021; Siebert and Reid 2023].

6.2 Volume of the VDAD

The volume of the excavated debris transported is obscured and challenging to calculate from the onshore scar dimensions alone because much of Heard Island is covered by glaciers. Using multibeam data, we show the minimum submarine area of this landslide deposit covers at least 467 km^2. Although it is likely the deposit extends beyond the limited surveyed region, particularly in the inferred southwest failure direction, where the seafloor steeply deepens from ~100 m on the Central Kerguelen Plateau to over 1000 m (Figure 1B, 1C, and Figure 3A). We suggest that our estimated 467 km^2 area of the VDAD is likely to be a minimum size estimate of the true deposit boundaries for two reasons: (1) the data resolution cannot detect blocks or features smaller than four-cell sizes (i.e. 20 m), meaning that the finer debris transported along with the larger blocky debris is not resolvable using ship-mounted multibeam, (2) the limited swath coverage provides only a few locations where we can define the boundaries of the VDAD, and there may be unaccounted for debris deposited beyond the mapped region.

Although it is difficult to estimate VDAD thickness without subsurface information, Profile A–A' (Figure 4B) suggests the minimum deposit thickness is ~60 m (excluding rafted blocks) and the maximum thickness (including blocks) is ~120 m. The resulting range of approximate deposit volumes based on spatial measurements in this study is between 14–28 km^3 (where, volume = (area × thickness)/2). It is important to note that the deposit thickness is highly variable across the mapped region (Figure 4B), with little known about the distribution of finer debris below the limits of detection of these datasets. This is consistent with observations of other (non-volcanic) mass-transport deposits globally, where deposit thickness is documented to be a poor indicator of landslide size due to lateral variation [Moscardelli and Wood 2015]. The observable size (area and length) of the Heard Island VDAD as measured from available multibeam data, fits within the highly variable dimensions of other documented submarine landslides from intraplate volcanic islands globally (Figure 8) [Blahůt et al. 2019]. However, a more comprehensive and targeted marine geophysical survey is required to improve volume estimates and reconstruct VDAD geometry.

6.3 Timing of the Heard Island volcanic landslide

Determining the precise ages of pre-historic landslides is challenging due to a paucity of suitable material to analyse, and if the VDAD is geologically young, a limited number of suitable techniques available [Grosse et al. 2022]. Even the best age estimates for landslides typically yield minimum and maximum age ranges, representing the youngest and oldest possi-

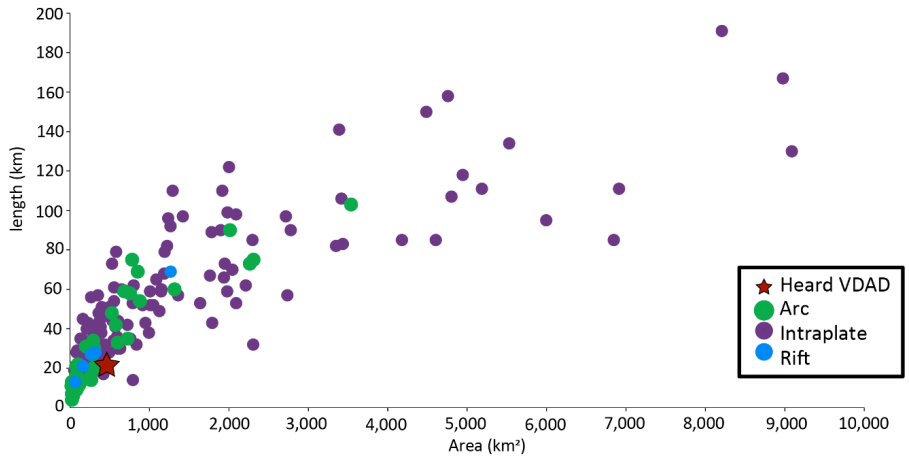

Figure 8: Plot of documented submarine landslide deposits from volcanic islands globally [Blahůt et al. 2019]. The dimensions of the Heard Island VDAD, as presented in this study, is shown by red star.

ble date range respectively for the landslide event(s) to have occurred [Urlaub et al. 2013]. Direct dating of landslides has been achieved by cosmogenic dating of the landslide surface or by $^{40}Ar/^{39}Ar$ dating of basal frictional melt zones [Legros et al. 2000; Jicha et al. 2015]. At Heard Island the opportunity to date the landslide surface is not available due to the landslide scar now being occupied by the Abbotsmith, Lied, and Gotley glaciers. We determined the $^{40}Ar/^{39}Ar$ ages of two Big Ben sourced lava clasts from within the VDAD. The youngest age, 18.0 ± 1.4 ka, represents an indirect maximum age for the landslide, assuming a single event. The landslide is younger than the undated Mawson Peak cone that overlaps the landslide scar [Stephenson et al. 2005]. There are no other dated or undated field relationships that would assist to refine the timing of the landslide further. The age of the landslide could be further refined by additional $^{40}Ar/^{39}Ar$ of the existing samples from the VDAD, collecting additional rocks samples from the VDAD for $^{40}Ar/^{39}Ar$ dating and ^{14}C dating of organic material in the VDAD sediments.

6.4 Potential factors that initiated the Heard Island volcanic landslide

Multiple events or processes can individually, or together, precondition a volcano for, and/or trigger a volcanic landslide [Delcamp et al. 2018; Roverato et al. 2021]. These include intrusion of shallow magmatic bodies (with or without eruption), evacuation of magma from the edifice (eruption or withdrawal), structural setting, slope instability, earthquakes, and climate change [Cas and Wright 1987; Carrasco-Núñez et al. 2011; Acocella 2021]. In the context of Big Ben, it is difficult to fully evaluate the role of most of these factors due to the extensive ice and snow cover and the paucity of relevant field observations.

Details regarding timing, frequency and styles of eruption at Big Ben are not well known making the role of magmatic and eruptive history in causing a volcanic landslide challenging to assess. The size and preservation of Big Ben has been interpreted to indicate an estimated age of onset of volcanic activity as ca. ≤1 Myr [Clarke et al. 1983]. However, the oldest of the small number of lava samples dated is 180 ± 18 ka [Duncan et al. 2016] (Figure 7C) indicating Big Ben could be much younger than this estimate although sampling is spatially biased due to ice cover. Volcanic sequences that are exposed comprise mainly layers of basaltic lavas with little evidence of intercalated pyroclastic deposits suggesting a predominantly effusive history. Historically, witnessed eruptions have been mainly low level effusive, and less commonly, low level explosive activity focussed at Mawson Peak [Fox et al. 2021]. The internal structure and plumbing system of Big Ben is unknown and there is no data to suggest past internal movement of magma has resulted in slope deformation or instability or existence of significant layers of pyroclastic deposits that could act as slide planes. The paucity of data means that magmatic and volcanic activity cannot be excluded as a factor in preconditioning or triggering a landslide.

Regionally, the Kerguelen Plateau, has been deformed by extension [Houtz et al. 1977; Coffin et al. 1986]. Extensional regimes provide a tectonic environment where normal and transcurrent faults can develop [Lagmay et al. 2000; Delcamp et al. 2015]. Slip on normal or transcurrent faults is implicated in initiating volcanic landslides with the transport direction of the landslide occurring perpendicular to the orientation of the fault e.g. Kīlauea, Hawai'i [Cannon et al. 2001; Yamazaki et al. 2021] and Mount Meru, Tanzania [Delcamp et al. 2015]. Inferred sub-parallel northwest-southeast striking faults on Heard Island together with the alignment of volcanic cones and vents and the broader geographic alignment of Big Ben and Laurens Peninsula suggests that there could be a structural control on the location of volcanism (Figure 1C) [Fox et al. 2021]. The volcanic landslide scar on Big Ben is oriented perpendicular to this alignment, as is predicted if the landslide was initiated by movement on one of these faults [Delcamp et al. 2015].

Slope instability at Heard Island could be the product of several processes including overloading of slopes with new lava, hydrothermalism, basal erosion by ocean waves, periglacial activity and glacial retreat in response to climate change. Average magma discharge rates at Heard Island are low

0.0002 km^3 yr^{-1} [Fox et al. 2021] but could have been higher at the time of the landslide, contributing to slope instability. Hydrothermalism at volcanoes weakens rock mass strength, pre-disposing steep slopes to failure [van Wyk de Vries et al. 2000; Heap et al. 2021]. There is scant evidence of hydrothermal activity at Big Ben. Historically, two short-lived, suspected episodes of hydrothermal activity have been reported on the lower flanks and fumaroles were reported at the summit of Mawson Peak in 1983 [Fox et al. 2021]. There are no reports of hydrothermally altered stratigraphy. However, interactions between lava and ice can produce hydrothermally altered lavas and clastic rocks; these could be present but obscured. Fumaroles [Stephenson et al. 2006] and submarine gas venting have been observed at McDonald Islands [Spain et al. 2020] providing evidence for at least one active hydrothermal system in the region. Heard Island is significantly impacted by dynamic erosion in response to the prevailing westerly winds and ocean currents [Green 2000; Kiernan and McConnell 2008]. If similar atmospheric and ocean conditions were present at the end of the LGM, the oblique orientation of the south coast of Big Ben to these winds and currents could have contributing to slope instability by undercutting the southern flank. The influence of periglacial processes on slope instability at Heard Island in the past is unknown but suspected to be minimal post LGM due to retention of extensive ice and glacier cover [Kiernan and McConnell 2008]. In present day, periglacial processes on Big Ben are active but somewhat limited due to the relatively small area of land exposed, the short exposure time (for most areas likely <200 yr), and the low altitudes and hence relatively high ambient air temperatures, where land is exposed [Kiernan and McConnell 2008].

The maximum age for the Heard Island volcanic landslide falls towards the end of the Last Glacial Maximum (LGM). Globally, significant volcanic landslides have occurred over the last 30 kyr, just after local glacial maxima that ended with rapid deglaciation [Capra 2006]. Deglaciation of volcanic edifices pre-disposes volcanoes to collapse due to the loss of ice buttressing, local de-loading and glacial isostatic adjustment induced seismicity [Capra et al. 2013; Conway et al. 2016]. Changes to fluid circulation and pore fluid pressure inside the edifice induced by glacial melt, increased humidity and rainfall can also create further slope instability during and after glacial retreat [Capra 2006]. Changes in sea level at the end of glacial maxima have also been implicated in causing volcanic landslides although there is no strong evidence for this in intraplate settings [McMurtry et al. 2004; Coussens et al. 2016; Roberti et al. 2020]. The southern hemisphere experienced rapid climate change at ca. 17.7 ka accompanied by significant synchronous glacial retreat in New Zealand and Patagonia and changes to ice distribution in Antarctica [McConnell et al. 2017]. During the LGM a grounded ice sheet extended 70 km to the north and west of Heard Island, and 30 km to the south and east, evidenced by well-developed cross-shelf troughs and moraines (Figure 1B) [Balco 2007; Hodgson et al. 2014]. The ice sheet has since retreated to onshore Heard Island where ~70 % of the land surface is covered in glaciers originating from the upper slopes of Big Ben and one glacier near the summit of Mt Dixon on Laurens Peninsula [Ruddell 2006].

Globally, evidence for a link between glacial/interglacial cycles and cycles of volcanic processes, including increased frequency and size of volcanic eruptions, exists in a range of tectonic settings (e.g. divergent boundary and mantle plume, Iceland [Van Vliet-Lanoë et al. 2019], continental intraplate, France and Germany [Nowell et al. 2006], and volcanic arc, Izu-Bonin Arc [Schindlbeck et al. 2018], Garabaldi Volcanic Belt, Canada [Wilson and Russell 2020], Southern Andean Volcanic Zone, Chile [Watt et al. 2013]). However, there is insufficient data to support this link for oceanic island intraplate mantle plume settings in general and Heard Island specifically. The known volcanic history of Heard Island and the glacial history of both Heard Island and the surrounding region is not sufficiently detailed to make robust conclusions regarding spatial or temporal links between the two. It is possible that the combination of the structural setting and rapid rates of deglaciation post the LGM initiated the Heard Island landslide. However, other contributing factors cannot be excluded based on the currently available data.

6.5 Past impacts of volcanic landslide at Heard Island

Volcanic landslides can trigger eruption, dissect and/or modify existing plumbing systems, and result in changes to lava composition [Guillou et al. 1998; Martínez et al. 2018; Watt 2019]. The current focus of volcanic activity at Heard Island, Mawson Peak, is offset from the centre of the pre-volcanic landslide summit crater and overlaps its margins and the landslide scar (Figure 3C), indicating post-landslide modification of the upper portion of Big Ben plumbing system and emergence of a new vent. Holocene pyroclastic cones around the coast of Heard Island are younger (1.9 ± 3.8 to 13.3 ± 4.1 ka) than the maximum age of the volcanic landslide and could reflect the emergence of new, relatively short-lived volcanic focal points post-collapse [Fox et al. 2021] but there remains insufficient data regarding the relative or absolute age of the landslide to support this interpretation. Changes to Big Ben lava composition post-volcanic landslide is not apparent with the available datasets [Stephenson 1972; Barling et al. 1994; Fox et al. 2021], however sampling is biased by ice cover.

Volcanic landslides in marine or lake settings can generate tsunami [Schindelé et al. 2024] (e.g. Mombacho, Nicaragua [Freundt et al. 2007], Stromboli, Italy [Tinti et al. 2006], and Anak Krakatau, Indonesia [Grilli et al. 2021]). The direction of transport of the Big Ben landslide together with its volume suggests that any tsunami generated could have reached Antarctica or other far field locations. A landslide of similar size on the northern flanks of Big Ben could generate tsunami that reaches the Kerguelen Islands or, if on the eastern flank, the southwest coast of Australia. The next step in assessing past and future impacts of volcanic landslide at Heard Island is to numerically model the tsunami that could have been produced by the volcanic landslide although this will be complicated by incomplete source and deposit volumes and the likely presence of ice blocks as well as rock in the debris avalanche material.

6.6 Future volcanic landslide risk at Heard Island

Assessing the future risk of landslide at Heard Island is challenging because there are characteristics of the island that are not typical of other oceanic island volcanoes and because not all potential pre-conditioning and triggering factors can be assessed (see discussion Section 6.4). Heard Island is unusual for an oceanic volcanic island in that there is only evidence for one significant volcanic landslide during its history ca. <1 Myr) [Clarke et al. 1983; Stephenson et al. 2005; Fox et al. 2021]. Hotspot volcanoes in the oceans have typically experienced multiple landslides during similar time frames (e.g. Réunion Island [Oehler et al. 2007], Canary Islands [Ferrer et al. 2021]). Heard Island is understudied and evidence for multiple landslide events may be revealed by collection of additional on-shore and off-shore data. Alternatively, there are characteristics of Heard Island's setting and volcanic evolution that may mean it is less vulnerable to frequent landslides than other hotspot volcanoes. Heard Island has a very low magma discharge rate of 0.0002 $km^3\ yr^{-1}$ [Fox et al. 2021] compared to other basaltic intraplate volcanic islands over the past million years e.g. Hawai'i (0.14–0.21 $km^3\ yr^{-1}$ [Jicha et al. 2012; Jourdan et al. 2012; Garcia et al. 2017]), Piton des Neiges, Réunion Island (0.01 $km^3\ yr^{-1}$ [de Voogd et al. 1999]), and Canary Islands (up to 1 $km^3\ yr^{-1}$ [Carracedo et al. 2007]). The low magma discharge rate at Heard Island does not produce overly loaded and unstable slopes that are seen at these locations and may account for the disparity in the frequency of landslides and reduce the risk of future volcanic landslide.

Heard Island is also atypical for islands arising from mantle hotspots that have experienced volcanic landslides because it is located in a relatively shallow (<200 m) marine environment on the Kerguelen Plateau and does not rise from abyssal depths. Despite its size, it has not subsided, but rather has been uplifted and nearly all Big Ben volcano is exposed above sea level [Stephenson et al. 2005; Fox et al. 2021]. The lack of gravitational potential offshore compared to all other islands created by mantle hotspots and the buttressing provided by glaciers [Pánek et al. 2021] likely decrease the vulnerability to volcanic landslide.

Heard Island is experiencing significant glacial retreat, potentially increasing the risk of future volcanic landslides. Glacial retreat on Heard Island has been accompanied by significant changes to subglacial streams and ice marginal processes which can enhance erosion and slope instability. In addition to exposing steep cliff faces, erosion rates can increase as meltwater volume and velocity increase. Although not well quantified, evidence for active changes in hydrology on Big Ben in response to glacier retreat includes expanding proglacial lagoons, widening and re-positioning of meltwater channels and streams, and changed sediment deposition and erosion patterns [Kiernan and McConnell 2002; Thost and Truffer 2008]. Future risk of slope instability and subsequent landslide at Big Ben can only increase if the current rate of glacial retreat continues.

Changes in atmospheric and oceanic circulation patterns in response to climate change concentrate heat in the high latitudes of the southern hemisphere [Roemmich et al. 2015; Gao et al. 2017; Bakke et al. 2021]. The relatively high rates of glacial retreat at Heard Island have been attributed to global climate change [Pendlebury and Barnes-Keoghan 2007]. Historical accounts and photographic evidence reveals that the glaciers on Heard Island were much larger in the recent past (ca. 1850s) when almost all Heard Island glaciers extended to the shoreline [Budd 2000]. Glacial retreat and thinning has accelerated over the past 30–50 years [Budd and Stephenson 1970; Allison and Keage 1986; Kiernan and McConnell 2002; Hall 2004] producing a >30 % reduction in the volume of the glaciers since that time [Ruddell 2006; Thost and Truffer 2008; Cogley et al. 2014]. Average temperatures in the sub-Antarctic have risen much more quickly than the global average and are forecast to continue to rise [Nel et al. 2023]. This has resulted in the long-term decline of glaciers in the sub-Antarctic including those on other sub-Antarctic volcanic islands [Cogley et al. 2014]. Further rising temperatures and subsequent glacial retreat will increase the risk of minor and major volcanic landslides on Heard Island and other volcanic islands in similar settings.

Data that would aid in a more quantitative assessment of future risk of volcanic landslide at Heard Island should be centred around understanding the past spatiotemporal distribution of seismicity, volcanism and ice, both at Heard Island and in the surrounding region, and the timing and number of past volcanic landslides at Heard Island. Full coverage of multibeam bathymetry data around Heard Island extending to areas of known or suspected glacial morphological features on the seafloor together with sediment coring of submerged moraines would help define regional ice extent and timing. On-shore, mapping of glacial geomorphology, ^{14}C dating of moraines and cosmogenic dating of glacial erratics and glacially striated bedrock would assist with assessing timing and extent of glacial retreat and advance. Additional work designed to resolve detail regarding the timing and types of volcanic events and processes (eruptions, hydrothermalism, volcanic landslide) will also be important.

7 Conclusions

This study provides the first geologic and geophysical evidence for a large VDAD offshore Heard Island, corresponding to an onshore scar on the southwestern flank of Big Ben volcano. The Heard Island landslide represents one of only very few documented km-scale volcanic landslide events within the sub-Antarctic zone and is an important morphological process in the evolution of Heard Island. Results show that the Heard Island landslide initiated on the subaerial portion of Big Ben volcano and transported blocky debris downslope, at least 21 km from the present-day coastline. The estimated volume of the submarine VDAD is between 14–28 km^3, which could have been deposited in one or multiple landslide events.

The new $^{40}Ar/^{39}Ar$ ages presented here (38.1 ± 4.1 ka and 18.0 ± 1.4 ka) provide the first maximum age, 18.0 ± 1.4 ka, for the previously un-dated Heard Island volcanic landslide. If the timing is contemporaneous with the end of the LGM, it suggests that de-glaciation could be a preconditioning or triggering factor for the landslide. Glacier retreat at Heard Island and elsewhere in the sub-Antarctic is predicted to continue in response to climate change and could result in increased

frequency of volcanic landslide and associated hazards. However, the structural setting of Heard Island may also be important and there is insufficient data to assess the influence of other contributing factors such as hydrothermal alteration, magmatic, and eruptive processes.

Although Heard Island lies within the remote southern Indian Ocean, a km-scale volcanic landslide, such as the one detailed in this study, may have generated tsunami able to reach distant coastlines. Numerical modelling of tsunami wave propagation triggered by this landslide would assist in understanding the potential far-field impacts, beyond morphological changes to the volcano and immediate surrounding seafloor.

Author Contributions

JF and SW are co-first authors having contributed equally to data collection, interpretation, and preparation of the first draft of the manuscript and are listed alphabetically. JF led sample processing on-board, conducted sample preparation, completed petrographical analyses, led interpretation of geochemical and geochronological data and co-wrote the first draft of the manuscript. SW contributed to on-board sample processing, hydroacoustic data acquisition and processing, led post-cruise bathymetric and digital elevation data processing and interpretation, and co-wrote the first draft of the manuscript. TF guided geochemistry data acquisition, geochemistry figures, geochemistry interpretations and revision of text and figures. RC and JW advised on research design, interpretation of results and contributed to revision of text and figures. ES contributed to on-board sample processing, hydroacoustic data acquisition and processing and to revision of text and figures. RD guided the interpretation of geochronology data and contributed to revision of text and figures. MC conceived and obtained ship time and funding for the overall research project, and MC and RA designed and led the research voyage and contributed to revision of text and figures.

Acknowledgements

This research was supported by a grant of sea time on RV Investigator from the CSIRO Marine National Facility (https://ror.org/01mae9353). We thank the captain, crew and fellow scientists of the RV *Investigator* voyage IN2016_V01. Analytical work was supported by Australian Antarctic Science Program (AASP) Grant 4338 (MC). JF is supported by a Japanese Society for the Promotion of Science Post-doctoral Fellowship. We thank H. Guillou and an anonymous reviewer whose constructive suggestions helped improve the manuscript.

Data Availability

All supporting geochemical and geochronology data is included in the text and supplementary materials. Bathymetric data is available via the Australian CSIRO Data Collection https://doi.org/10.25919/jw5f-ad35.

Copyright Notice

References

Acocella, V. (2021). "Volcano Flank Instability and Collapse". *Volcano-Tectonic Processes*. Springer International Publishing, pages 205–244. ISBN: 9783030659684. DOI: 10.1007/978-3-030-65968-4_6.

Allison, I. F. and P. L. Keage (1986). "Recent changes in the glaciers of Heard Island". *Polar Record* 23(144), pages 255–272. DOI: 10.1017/S0032247400007099.

Bakke, J., Ø. Paasche, J. M. Schaefer, and A. Timmermann (2021). "Long-term demise of sub-Antarctic glaciers modulated by the Southern Hemisphere Westerlies". *Scientific Reports* 11 (8361), page 8361. DOI: 10.1038/s41598-021-87317-5.

Balco, G. (2007). "A surprisingly large marine ice cap at Heard Island during the Last Glacial Maximum?" *U.S. Geological Survey Open-File Report* (2007-1047), page 147.

Barling, J. (1994). "Origin and evolution of a high-Ti ocean island basalt suite: The Laurens Peninsula Series, Heard Island, Indian Ocean". *Goldschmidt Conference Edinburgh*. Volume 58A. Mineralogical Magazine, pages 49–50.

Barling, J., S. L. Goldstein, and I. A. Nicholls (1994). "Geochemistry of Heard Island (Southern Indian Ocean): Characterization of an Enriched Mantle Component and Implications for Enrichment of the Sub-Indian Ocean Mantle". *Journal of Petrology* 35 (4), pages 1017–1053. DOI: 10.1093/petrology/35.4.1017.

Beaman, R. and P. O'Brien (2011). "Kerguelen Plateau Bathymetric Grid, November 2010". *Geoscience Australia, Canberra*. [Record].

Beaman, R. (2023). "AusBathyTopo (Kerguelen Plateau) 100m 2022 - A high-resolution depth model (20220004C)". *Geoscience Australia, Canberra*. DOI: 10.26186/147703. [Dataset].

Bell, K. L. C., S. N. Carey, P. Nomikou, H. Sigurdsson, and D. Sakellariou (2013). "Submarine evidence of a debris avalanche deposit on the eastern slope of Santorini volcano, Greece". *Tectonophysics* 597–598, pages 147–160. DOI: 10.1016/j.tecto.2012.05.006.

Bernard, B., S. Takarada, S. D. Andrade, and A. Dufresne (2021). "Terminology and Strategy to Describe Large Volcanic Landslides and Debris Avalanches". *Volcanic Debris Avalanches*. Edited by M. Roverato, A. Dufresne, and J. Procter. Springer International Publishing, pages 51–73. ISBN: 9783030574116. DOI: 10.1007/978-3-030-57411-6_3.

Blahůt, J., J. Balek, J. Klimeš, M. Rowberry, M. Kusák, and J. Kalina (2019). "A comprehensive global database of giant landslides on volcanic islands". *Landslides* 16(10), pages 2045–2052. DOI: 10.1007/s10346-019-01275-8.

Budd, G. M. (2000). "Changes in Heard Island glaciers, king penguins and fur seals since 1947". *Papers and Proceedings*

of the Royal Society of Tasmania 133, pages 47–60. DOI: 10.26749/rstpp.133.2.47.

Budd, G. and P. Stephenson (1970). "Recent glacier retreat on Heard Island". *International Symposium on Antarctic Glaciological Exploration, Hanover NH, 1968*. Edited by A. J. Gow, C. Keeler, C. C. Langway, and W. F. Weeks. Volume 86. International Association of Scientific Hydrology, pages 449–458.

Cannon, E. C., R. Bürgmann, and S. Owen (2001). "Shallow Normal Faulting and Block Rotation Associated with the 1975 Kalapana Earthquake, Kilauea Volcano, Hawaii". *Bulletin of the Seismological Society of America* 91(6), pages 1553–1562. DOI: 10.1785/0120000072.

Capra, L. (2006). "Abrupt climatic changes as triggering mechanisms of massive volcanic collapses". *Journal of Volcanology and Geothermal Research* 155(3–4), pages 329–333. DOI: 10.1016/j.jvolgeores.2006.04.009.

Capra, L., J. P. Bernal, G. Carrasco-Núñez, and M. Roverato (2013). "Climatic fluctuations as a significant contributing factor for volcanic collapses. Evidence from Mexico during the Late Pleistocene". *Global and Planetary Change* 100, pages 194–203. DOI: 10.1016/j.gloplacha.2012.10.017.

Capra, L., J. L. Macías, K. M. Scott, M. Abrams, and V. H. Garduño-Monroy (2002). "Debris avalanches and debris flows transformed from collapses in the Trans-Mexican Volcanic Belt, Mexico – behavior, and implications for hazard assessment". *Journal of Volcanology and Geothermal Research* 113(1–2), pages 81–110. DOI: 10.1016/s0377-0273(01)00252-9.

Carracedo, J. C., E. R. Badiola, H. Guillou, M. Paterne, S. Scaillet, F. . P. Torrado, R. Paris, U. Fra-Paleo, and A. Hansen (2007). "Eruptive and structural history of Teide Volcano and rift zones of Tenerife, Canary Islands". *GSA Bulletin* 119(9–10), pages 1027–1051. DOI: 10.1130/b26087.1.

Carracedo, J. C., H. Guillou, S. Nomade, E. Rodríguez-Badiola, F. J. Pérez-Torrado, A. Rodríguez-González, R. Paris, V. R. Troll, S. Wiesmaier, A. Delcamp, and J. L. Fernandez-Turiel (2010). "Evolution of ocean-island rifts: The northeast rift zone of Tenerife, Canary Islands". *GSA Bulletin* 123(3–4), pages 562–584. DOI: 10.1130/b30119.1.

Carrasco-Núñez, G., L. Siebert, and L. Capra (2011). "Hazards from volcanic avalanches". *Horizons in Earth Science Research* 3, pages 199–227.

Carter, B. A., R. Pradipta, T. Dao, J. L. Currie, S. Choy, P. Wilkinson, P. Maher, R. Marshall, K. Harima, M. Le Huy, T. Nguyen Chien, T. Nguyen Ha, and T. J. Harris (2023). "The Ionospheric Effects of the 2022 Hunga Tonga Volcano Eruption and the Associated Impacts on GPS Precise Point Positioning Across the Australian Region". *Space Weather* 21(5), e2023SW003476. DOI: 10.1029/2023sw003476.

Cas, R. and J. Wright (1987). *Volcanic successions: modern and ancient*. Springer Dordrecht. 528 pages. ISBN: 978-94-009-3167-1. DOI: 10.1007/978-94-009-3167-1.

Clarke, I., I. MacDougall, and D. Whitford (1983). "Volcanic evolution of Heard and McDonald islands, southern Indian Ocean". *Antarctic Earth Science*. Edited by P. R. J. R. L. Oliver and J. B. Jago. Cambridge University Press, pages 631–635. ISBN: 9780521183796.

Coffin, M., F. Cooke, T. Martin, M. Boyd, and C. Navidad (2023). "IN2016_V01 Heard and Macdonald Islands Bathymetry 10m - 210m Multi-resultion AusSeabed products, v2". *CSIRO*. DOI: 10.25919/jw5f-ad35. [Dataset].

Coffin, M. F., H. L. Davies, and W. F. Haxby (1986). "Structure of the Kerguelen Plateau province from Seasat altimetry and seismic reflection data". *Nature* 324(6093), pages 134–136. DOI: 10.1038/324134a0.

Coffin, M. F., M. S. Pringle, R. A. Duncan, T. P. Gladczenko, M. Storey, R. D. Müller, and L. A. Gahagan (2002). "Kerguelen Hotspot Magma Output since 130 Ma". *Journal of Petrology* 43(7), pages 1121–1137. DOI: 10.1093/petrology/43.7.1121.

Cogley, J. G., E. Berthier, and S. Donoghue (2014). "Remote Sensing of Glaciers of the Subantarctic Islands". *Global Land Ice Measurements from Space*. Edited by J. Kargel, G. Leonard, M. Bishop, A. Kääb, and B. Raup. Springer Berlin Heidelberg, pages 759–780. ISBN: 9783540798187. DOI: 10.1007/978-3-540-79818-7_32.

Conway, C. E., G. S. Leonard, D. B. Townsend, A. T. Calvert, C. J. Wilson, J. A. Gamble, and S. R. Eaves (2016). "A high-resolution $^{40}Ar/^{39}Ar$ lava chronology and edifice construction history for Ruapehu volcano, New Zealand". *Journal of Volcanology and Geothermal Research* 327, pages 152–179. DOI: 10.1016/j.jvolgeores.2016.07.006.

Coussens, M., D. Wall-Palmer, P. J. Talling, S. F. L. Watt, M. Cassidy, M. Jutzeler, M. A. Clare, J. E. Hunt, M. Manga, T. M. Gernon, M. R. Palmer, S. J. Hatter, G. Boudon, D. Endo, A. Fujinawa, R. Hatfield, M. J. Hornbach, O. Ishizuka, K. Kataoka, A. Le Friant, F. Maeno, M. McCanta, and A. J. Stinton (2016). "The relationship between eruptive activity, flank collapse, and sea level at volcanic islands: A long-term (>1 Ma) record offshore Montserrat, Lesser Antilles". *Geochemistry, Geophysics, Geosystems* 17(7), pages 2591–2611. DOI: 10.1002/2015gc006053.

Delcamp, A., D. Delvaux, S. Kwelwa, A. Macheyeki, and M. Kervyn (2015). "Sector collapse events at volcanoes in the North Tanzanian divergence zone and their implications for regional tectonics". *Geological Society of America Bulletin*, B31119.1. DOI: 10.1130/b31119.1.

Delcamp, A., S. Poppe, M. Detienne, and E. Paguican (2018). "Destroying a Volcanic Edifice—Interactions Between Edifice Instabilities and the Volcanic Plumbing System". *Volcanic and Igneous Plumbing Systems*. Edited by S. Burchardt. Elsevier, pages 231–257. ISBN: 9780128097496. DOI: 10.1016/b978-0-12-809749-6.00009-1.

De Voogd, B., S. P. Palomé, A. Hirn, P. Charvis, J. Gallart, D. Rousset, J. Dañobeitia, and H. Perroud (1999). "Vertical movements and material transport during hotspot activity: Seismic reflection profiling offshore La Réunion". *Journal of Geophysical Research: Solid Earth* 104(B2), pages 2855–2874. DOI: 10.1029/98jb02842.

Dufresne, A., A. Zernack, K. Bernard, J.-C. Thouret, and M. Roverato (2021). "Sedimentology of Volcanic Debris Avalanche Deposits". *Volcanic Debris Avalanches*. Edited by M. Roverato, A. Dufresne, and J. Procter. Springer International Publishing, pages 175–210. ISBN: 9783030574116. DOI: 10.1007/978-3-030-57411-6_8.

Duncan, R. A., P. G. Quilty, J. Barling, and J. M. Fox (2016). "Geological development of Heard Island, Central Kerguelen Plateau". *Australian Journal of Earth Sciences* 63(1), pages 81–89. DOI: 10.1080/08120099.2016.1139000.

Ferrer, M., L. González de Vallejo, J. Madeira, C. Andrade, J. C. García-Davalillo, M. d. C. Freitas, J. Meco, J. F. Betancort, T. Torres, and J. E. Ortiz (2021). "Megatsunamis Induced by Volcanic Landslides in the Canary Islands: Age of the Tsunami Deposits and Source Landslides". *GeoHazards* 2(3), pages 228–256. DOI: 10.3390/geohazards2030013.

Fleck, R. J., J. F. Sutter, and D. H. Elliot (1977). "Interpretation of discordant $^{40}Ar/^{39}Ar$ age-spectra of mesozoic tholeiites from antarctica". *Geochimica et Cosmochimica Acta* 41(1), pages 15–32. DOI: 10.1016/0016-7037(77)90184-3.

Fox, J. M., J. McPhie, R. J. Carey, F. Jourdan, and D. P. Miggins (2021). "Construction of an intraplate island volcano: The volcanic history of Heard Island". *Bulletin of Volcanology* 83(5), page 37. DOI: 10.1007/s00445-021-01452-5.

Freundt, A., W. Strauch, S. Kutterolf, and H.-U. Schmincke (2007). "Volcanogenic Tsunamis in Lakes: Examples from Nicaragua and General Implications". *Pure and Applied Geophysics* 164(2–3), pages 527–545. DOI: 10.1007/s00024-006-0178-z.

Gao, L., S. R. Rintoul, and W. Yu (2017). "Recent wind-driven change in Subantarctic Mode Water and its impact on ocean heat storage". *Nature Climate Change* 8(1), pages 58–63. DOI: 10.1038/s41558-017-0022-8.

Garcia, M. O., B. R. Jicha, J. P. Marske, and A. J. Pietruszka (2017). "How old is Kīlauea Volcano (Hawai'i)? Insights from $^{40}Ar/^{39}Ar$ dating of the 1.7-km-deep SOH-1 core". *Geology* 45(1), pages 79–82. DOI: 10.1130/g38419.1.

GEBCO Bathymetric Compilation Group 2023 (2023). "The GEBCO_2023 Grid - a continuous terrain model of the global oceans and land". DOI: 10.5285/f98b053b-0cbc-6c23-e053-6c86abc0af7b.

Glicken, H. (1991). "Sedimentary architecture of large volcanic-debris avalanches". *Sedimentation in Volcanic Settings*. Edited by R. Fisher and G. Smith. SEPM Society for Sedimentary Geology, pages 99–106. ISBN: 0918985927. DOI: 10.2110/pec.91.45.0099.

Green, K. (2000). "Coastal studies at Heard Island 1992/93: changes in sea surface temperature and coastal landforms". *Papers and Proceedings of the Royal Society of Tasmania* 133, pages 27–32. DOI: 10.26749/rstpp.133.2.27.

Grilli, S., C. Zhang, J. Kirby, A. Grilli, D. Tappin, S. Watt, J. Hunt, A. Novellino, S. Engwell, M. Nurshal, M. Abdurrachman, M. Cassidy, A. Madden-Nadeau, and S. Day (2021). "Modeling of the Dec. 22nd 2018 Anak Krakatau volcano lateral collapse and tsunami based on recent field surveys: Comparison with observed tsunami impact". *Marine Geology* 440, page 106566. DOI: 10.1016/j.margeo.2021.106566.

Grosse, P., M. Danišík, F. D. Apaza, S. R. Guzmán, P. Lahitte, X. Quidelleur, S. Self, C. Siebe, B. van Wyk de Vries, G. Ureta, M. Guillong, R. De Rosa, P. Le Roux, J.-F. Wotzlaw, and O. Bachmann (2022). "Holocene collapse of Socompa volcano and pre- and post-collapse growth rates constrained by multi-system geochronology". *Bulletin of Volcanology* 84(9), page 85. DOI: 10.1007/s00445-022-01594-0.

Guillou, H., J. C. Carracedo, and S. J. Day (1998). "Dating of the Upper Pleistocene–Holocene volcanic activity of La Palma using the unspiked K–Ar technique". *Journal of Volcanology and Geothermal Research* 86(1–4), pages 137–149. DOI: 10.1016/s0377-0273(98)00074-2.

Hall, K. (2004). "Quaternary glaciation of the sub-Antarctic Islands". *Developments in Quaternary Sciences*. Edited by J. Ehlers and P. Gibbard. Elsevier BV, pages 339–345. DOI: 10.1016/S1571-0866(04)80140-4.

Heap, M. J., T. S. Baumann, M. Rosas-Carbajal, J.-C. Komorowski, H. A. Gilg, M. Villeneuve, R. Moretti, P. Baud, L. Carbillet, C. Harnett, and T. Reuschlé (2021). "Alteration-Induced Volcano Instability at La Soufrière de Guadeloupe (Eastern Caribbean)". *Journal of Geophysical Research: Solid Earth* 126(8), e2021JB022514. DOI: 10.1029/2021jb022514.

Hodgson, D. A., A. G. Graham, S. J. Roberts, M. J. Bentley, C. Ó. Cofaigh, E. Verleyen, W. Vyverman, V. Jomelli, V. Favier, D. Brunstein, D. Verfaillie, E. A. Colhoun, K. M. Saunders, P. M. Selkirk, A. Mackintosh, D. W. Hedding, W. Nel, K. Hall, M. S. McGlone, N. Van der Putten, W. A. Dickens, and J. A. Smith (2014). "Terrestrial and submarine evidence for the extent and timing of the Last Glacial Maximum and the onset of deglaciation on the maritime-Antarctic and sub-Antarctic islands". *Quaternary Science Reviews* 100, pages 137–158. DOI: 10.1016/j.quascirev.2013.12.001.

Houtz, R. E., D. E. Hayes, and R. G. Markl (1977). "Kerguelen Plateau bathymetry, sediment distribution and crustal structure". *Marine Geology* 25(1–3), pages 95–130. DOI: 10.1016/0025-3227(77)90049-4.

Hunt, J. E., D. R. Tappin, S. F. L. Watt, S. Susilohadi, A. Novellino, S. K. Ebmeier, M. Cassidy, S. L. Engwell, S. T. Grilli, M. Hanif, W. S. Priyanto, M. A. Clare, M. Abdurrachman, and U. Udrekh (2021). "Submarine landslide megablocks show half of Anak Krakatau island failed on December 22nd, 2018". *Nature Communications* 12(1), page 2827. DOI: 10.1038/s41467-021-22610-5.

Jicha, B. R., B. J. Laabs, J. M. Hora, B. S. Singer, and M. W. Caffee (2015). "Early Holocene collapse of Volcán Parinacota, central Andes, Chile: Volcanological and paleohydrological consequences". *Geological Society of America Bulletin* 127(11–12), pages 1681–1688. DOI: 10.1130/b31247.1.

Jicha, B. R., J. M. Rhodes, B. S. Singer, and M. O. Garcia (2012). "$^{40}Ar/^{39}Ar$ geochronology of submarine Mauna Loa volcano, Hawaii". *Journal of Geophysical Research: Solid Earth* 117(B9). DOI: 10.1029/2012jb009373.

Jourdan, F., W. D. Sharp, and P. R. Renne (2012). "$^{40}Ar/^{39}Ar$ ages for deep (3.3 km) samples from the Hawaii Scientific Drilling Project, Mauna Kea volcano, Hawaii". *Geochemistry, Geophysics, Geosystems* 13(5), Q05004. DOI: 10.1029/2011gc004017.

Kiernan, K. and A. McConnell (2008). "Periglacial processes on Heard Island, Southern Indian Ocean". *Papers and Proceedings of the Royal Society of Tasmania* 142, pages 1–12. DOI: 10.26749/rstpp.142.2.1.

Kiernan, K. and A. McConnell (1999). "Geomorphology of the Sub-Antarctic Australian Territory of Heard Island-McDonald Island". *Australian Geographer* 30(2), pages 159–195. DOI: 10.1080/00049189993693.

Kiernan, K. and A. McConnell (2002). "Glacier retreat and melt-lake expansion at Stephenson Glacier, Heard Island World Heritage Area". *Polar Record* 38(207), pages 297–308. DOI: 10.1017/s0032247400017988.

Koppers, A. A. P., H. Staudigel, and R. A. Duncan (2003). "High-resolution $^{40}Ar/^{39}Ar$ dating of the oldest oceanic basement basalts in the western Pacific basin". *Geochemistry, Geophysics, Geosystems* 4(11), page 8914. DOI: 10.1029/2003gc000574.

Koppers, A. A. (2002). "ArArCALC—software for $^{40}Ar/^{39}Ar$ age calculations". *Computers & Geosciences* 28(5), pages 605–619. DOI: 10.1016/s0098-3004(01)00095-4.

Krastel, S., H.-U. Schmincke, C. L. Jacobs, R. Rihm, T. P. Le Bas, and B. Alibés (2001). "Submarine landslides around the Canary Islands". *Journal of Geophysical Research: Solid Earth* 106(B3), pages 3977–3997. DOI: 10.1029/2000jb900413.

Kuiper, K. F., A. Deino, F. J. Hilgen, W. Krijgsman, P. R. Renne, and J. R. Wijbrans (2008). "Synchronizing Rock Clocks of Earth History". *Science* 320(5875), pages 500–504. DOI: 10.1126/science.1154339.

Labazuy, P. (1996). "Recurrent landslides events on the submarine flank of Piton de la Fournaise volcano (Reunion Island)". *Geological Society, London, Special Publications* 110(1), pages 295–306. DOI: 10.1144/gsl.sp.1996.110.01.23.

Lagmay, A. M. F., B. van Wyk de Vries, N. Kerle, and D. M. Pyle (2000). "Volcano instability induced by strike-slip faulting". *Bulletin of Volcanology* 62(4–5), pages 331–346. DOI: 10.1007/s004450000103.

Lambeth, A. J. (1952). "A geological account of Heard island". *Journal and Proceedings of the Royal Society of New South Wales* 86, pages 14–19.

Le Maitre, R., P. Bateman, A. Dubek, J. Keller, J. Lameyre, A. Streckeisen, A. Wooley, and B. Zanettin (2002). *Igneous Rocks: A Classification and Glossary of Terms*. Cambridge University Press. ISBN: 9780511535581. DOI: 10.1017/cbo9780511535581.

Lee, J.-Y., K. Marti, J. P. Severinghaus, K. Kawamura, H.-S. Yoo, J. B. Lee, and J. S. Kim (2006). "A redetermination of the isotopic abundances of atmospheric Ar". *Geochimica et Cosmochimica Acta* 70(17), pages 4507–4512. DOI: 10.1016/j.gca.2006.06.1563.

Legros, F., J.-M. Cantagrel, and B. Devouard (2000). "Pseudotachylyte (Frictionite) at the Base of the Arequipa Volcanic Landslide Deposit (Peru): Implications for Emplacement Mechanisms". *The Journal of Geology* 108(5), pages 601–611. DOI: 10.1086/314421.

Lynett, P., M. McCann, Z. Zhou, W. Renteria, J. Borrero, D. Greer, O. Fa'anunu, C. Bosserelle, B. Jaffe, S. La Selle, A. Ritchie, A. Snyder, B. Nasr, J. Bott, N. Graehl, C. Synolakis, B. Ebrahimi, and G. E. Cinar (2022). "Diverse tsunamigenesis triggered by the Hunga Tonga-Hunga Ha'apai eruption". *Nature* 609(7928), pages 728–733. DOI: 10.1038/s41586-022-05170-6.

Maas, R., M. B. Kamenetsky, A. V. Sobolev, V. S. Kamenetsky, and N. V. Sobolev (2005). "Sr, Nd, and Pb isotope evidence for a mantle origin of alkali chlorides and carbonates in the Udachnaya kimberlite, Siberia". *Geology* 33(7), pages 549–552. DOI: 10.1130/g21257.1.

MacDonald, G. A. and T. Katsura (1964). "Chemical Composition of Hawaiian Lavas". *Journal of Petrology* 5(1), pages 82–133. DOI: 10.1093/petrology/5.1.82.

Martínez, P., B. S. Singer, H. M. Roa, and B. R. Jicha (2018). "Volcanologic and petrologic evolution of Antuco-Sierra Velluda, Southern Andes, Chile". *Journal of Volcanology and Geothermal Research* 349, pages 392–408. DOI: 10.1016/j.jvolgeores.2017.11.026.

Masson, D., A. Watts, M. Gee, R. Urgeles, N. Mitchell, T. Le Bas, and M. Canals (2002). "Slope failures on the flanks of the western Canary Islands". *Earth-Science Reviews* 57(1–2), pages 1–35. DOI: 10.1016/s0012-8252(01)00069-1.

McConnell, J. R., A. Burke, N. W. Dunbar, P. Köhler, J. L. Thomas, M. M. Arienzo, N. J. Chellman, O. J. Maselli, M. Sigl, J. F. Adkins, D. Baggenstos, J. F. Burkhart, E. J. Brook, C. Buizert, J. Cole-Dai, T. J. Fudge, G. Knorr, H.-F. Graf, M. M. Grieman, N. Iverson, K. C. McGwire, R. Mulvaney, G. Paris, R. H. Rhodes, E. S. Saltzman, J. P. Severinghaus, J. P. Steffensen, K. C. Taylor, and G. Winckler (2017). "Synchronous volcanic eruptions and abrupt climate change 17.7 ka plausibly linked by stratospheric ozone depletion". *Proceedings of the National Academy of Sciences* 114(38), pages 10035–10040. DOI: 10.1073/pnas.1705595114.

McGuire, W. J. (1996). "Volcano instability: a review of contemporary themes". *Geological Society, London, Special Publications* 110(1), pages 1–23. DOI: 10.1144/gsl.sp.1996.110.01.01.

McMurtry, G. M., P. Watts, G. J. Fryer, J. R. Smith, and F. Imamura (2004). "Giant landslides, mega-tsunamis, and paleo-sea level in the Hawaiian Islands". *Marine Geology* 203(3–4), pages 219–233. DOI: 10.1016/s0025-3227(03)00306-2.

Min, K., R. Mundil, P. R. Renne, and K. R. Ludwig (2000). "A test for systematic errors in $^{40}Ar/^{39}Ar$ geochronology through comparison with U/Pb analysis of a 1.1-Ga rhyolite". *Geochimica et Cosmochimica Acta* 64(1), pages 73–98. DOI: 10.1016/s0016-7037(99)00204-5.

Moore, J. G., W. B. Bryan, M. H. Beeson, and W. R. Normark (1995). "Giant blocks in the South Kona landslide, Hawaii". *Geology* 23(2), page 125. DOI: 10.1130/0091-7613(1995)023<0125:gbitsk>2.3.co;2.

Moore, J. G., W. R. Normark, and R. T. Holcomb (1994). "Giant Hawaiian landslides". *Annual Review of Earth and Planetary Sciences* 22(1), pages 119–144. DOI: 10.1146/annurev.ea.22.050194.001003.

Moscardelli, L. and L. Wood (2015). "Morphometry of mass-transport deposits as a predictive tool". *Geological Society of America Bulletin*, B31221.1. DOI: 10.1130/b31221.1.

Münker, C., S. Weyer, E. Scherer, and K. Mezger (2001). "Separation of high field strength elements (Nb, Ta, Zr, Hf) and Lu from rock samples for MC-ICPMS measurements". *Geo-*

chemistry, Geophysics, Geosystems 2(12). DOI: 10.1029/2001gc000183.

Nel, W., D. W. Hedding, and E. M. Rudolph (2023). "The sub-Antarctic islands are increasingly warming in the 21st century". *Antarctic Science* 35(2), pages 124–126. DOI: 10.1017/s0954102023000056.

Nowell, D. A. G., M. C. Jones, and D. M. Pyle (2006). "Episodic Quaternary volcanism in France and Germany". *Journal of Quaternary Science* 21(6), pages 645–675. DOI: 10.1002/jqs.1005.

Oehler, J.-F., J.-F. Lénat, and P. Labazuy (2007). "Growth and collapse of the Reunion Island volcanoes". *Bulletin of Volcanology* 70(6), pages 717–742. DOI: 10.1007/s00445-007-0163-0.

Pánek, T., M. Březný, J. Kilnar, and D. Winocur (2021). "Complex causes of landslides after ice sheet retreat: Post-LGM mass movements in the Northern Patagonian Icefield region". *Science of The Total Environment* 758, page 143684. DOI: 10.1016/j.scitotenv.2020.143684.

Pendlebury, S. and I. P. Barnes-Keoghan (2007). "Climate and climate change in the sub-Antarctic". *Papers and Proceedings of the Royal Society of Tasmania*, pages 67–81. DOI: 10.26749/rstpp.141.1.67.

Pin, C., A. Gannoun, and A. Dupont (2014). "Rapid, simultaneous separation of Sr, Pb, and Nd by extraction chromatography prior to isotope ratios determination by TIMS and MC-ICP-MS". *Journal of Analytical Atomic Spectrometry* 29(10), pages 1858–1870. DOI: 10.1039/c4ja00169a.

Quilty, P. (2007). "Origin and evolution of the sub-Antarctic islands: the foundation". *Papers and Proceedings of the Royal Society of Tasmania* 141, pages 35–58. DOI: 10.26749/rstpp.141.1.35.

Quilty, P. and G. Wheller (2000). "Heard Island and the McDonald Islands: a window into the Kerguelen Plateau". *Papers and Proceedings of the Royal Society of Tasmania* 133, pages 1–12. DOI: 10.26749/rstpp.133.2.1.

Roberti, G., N. J. Roberts, and C. Lit (2020). "Climatic Influence on Volcanic Landslides". *Volcanic Debris Avalanches*. Springer International Publishing, pages 121–141. ISBN: 9783030574116. DOI: 10.1007/978-3-030-57411-6_6.

Roemmich, D., J. Church, J. Gilson, D. Monselesan, P. Sutton, and S. Wijffels (2015). "Unabated planetary warming and its ocean structure since 2006". *Nature Climate Change* 5(3), pages 240–245. DOI: 10.1038/nclimate2513.

Roverato, M., F. Di Traglia, J. Procter, E. Paguican, and A. Dufresne (2021). "Factors Contributing to Volcano Lateral Collapse". *Volcanic Debris Avalanches*. Edited by M. Roverato, A. Dufresne, and J. Procter. Springer International Publishing, pages 91–119. ISBN: 9783030574116. DOI: 10.1007/978-3-030-57411-6_5.

Rowberry, M., J. Klimeš, J. Blahůt, J. Balek, and M. Kusák (2023). "A Global Database of Giant Landslides on Volcanic Islands". *Progress in Landslide Research and Technology*. Edited by K. Sassa, K. Konagai, Ž. Tiwari B. Arbanas, and S. Sassa. Springer International Publishing, pages 295–304. ISBN: 9783031168987. DOI: 10.1007/978-3-031-16898-7_22.

Ruddell, A. (2006). "An inventory of present glaciers on Heard Island and their historical variation". *Heard Island: Southern Ocean sentinel*. Edited by K. Green and E. Woehler. Chipping Norton, NSW: Surrey Beatty. ISBN: 0949324981.

Schaen, A. J., B. R. Jicha, K. V. Hodges, P. Vermeesch, M. E. Stelten, C. M. Mercer, D. Phillips, T. A. Rivera, F. Jourdan, E. L. Matchan, S. R. Hemming, L. E. Morgan, S. P. Kelley, W. S. Cassata, M. T. Heizler, P. M. Vasconcelos, J. A. Benowitz, A. A. Koppers, D. F. Mark, E. M. Niespolo, C. J. Sprain, W. E. Hames, K. F. Kuiper, B. D. Turrin, P. R. Renne, J. Ross, S. Nomade, H. Guillou, L. E. Webb, B. A. Cohen, A. T. Calvert, N. Joyce, M. Ganerød, J. Wijbrans, O. Ishizuka, H. He, A. Ramirez, J. A. Pfänder, M. Lopez-Martínez, H. Qiu, and B. S. Singer (2021). "Interpreting and reporting 40Ar/39Ar geochronologic data". *GSA Bulletin* 133(3–4), pages 461–487. DOI: 10.1130/b35560.1.

Schindelé, F., L. Kong, E. M. Lane, R. Paris, M. Ripepe, V. Titov, and R. Bailey (2024). "A Review of Tsunamis Generated by Volcanoes (TGV) Source Mechanism, Modelling, Monitoring and Warning Systems". *Pure and Applied Geophysics* 181(6), pages 1745–1792. DOI: 10.1007/s00024-024-03515-y.

Schindlbeck, J. C., M. Jegen, A. Freundt, S. Kutterolf, S. M. Straub, M. J. Mleneck-Vautravers, and J. F. McManus (2018). "100- kyr cyclicity in volcanic ash emplacement: evidence from a 1.1Myr tephra record from the NW Pacific". *Scientific Reports* 8(1). DOI: 10.1038/s41598-018-22595-0.

Siebert, L. (1984). "Large volcanic debris avalanches: Characteristics of source areas, deposits, and associated eruptions". *Journal of Volcanology and Geothermal Research* 22(3–4), pages 163–197. DOI: 10.1016/0377-0273(84)90002-7.

Siebert, L. and M. E. Reid (2023). "Lateral edifice collapse and volcanic debris avalanches: a post-1980 Mount St. Helens perspective". *Bulletin of Volcanology* 85(11). DOI: 10.1007/s00445-023-01662-z.

Spain, E. A., S. C. Johnson, B. Hutton, J. M. Whittaker, V. Lucieer, S. J. Watson, J. M. Fox, J. Lupton, R. Arculus, A. Bradney, and M. F. Coffin (2020). "Shallow Seafloor Gas emissions Near Heard and McDonald Islands on the Kerguelen Plateau, Southern Indian Ocean". *Earth and Space Science* 7(3). DOI: 10.1029/2019ea000695.

Steiger, R. and E. Jäger (1977). "Subcommission on geochronology: Convention on the use of decay constants in geo- and cosmochronology". *Earth and Planetary Science Letters* 36(3), pages 359–362. DOI: 10.1016/0012-821x(77)90060-7.

Stephenson, J., G. Budd, J. Manning, and P. Hansbro (2005). "Major eruption-induced changes to the McDonald Islands, southern Indian Ocean". *Antarctic Science* 17(2), pages 259–266. DOI: 10.1017/s095410200500266x.

Stephenson, P. (1964). "Some geological observations on Heard island". *Antarctic Geology - Proceedings of the First International Symposium on Antarctic Geology*. Edited by R. Adie. North-Holland Publishing Company, pages 14–24.

– (1972). "Geochemistry of some Heard Island igneous rocks". *Oslo: Universitetsforlaget*. Edited by R. Adie, pages 793–801.

Stephenson, P., J. Barling, G. Wheller, and I. Clarke (2006). "The geology and volcanic geomorphology of Heard Island". *Heard Island: Southern Ocean sentinel*. Edited by K. Green and E. Woehler. Chipping Norton, NSW: Surrey Beatty. ISBN: 0949324981.

Taylor, J. (1997). *Introduction to Error Analysis, the Study of Uncertainties in Physical Measurements*. University Science Books. ISBN: 9780935702750.

Thost, D. E. and M. Truffer (2008). "Glacier Recession on Heard Island, Southern Indian Ocean". *Arctic, Antarctic, and Alpine Research* 40(1), pages 199–214. DOI: 10.1657/1523-0430(06-084)[thost]2.0.co;2.

Tinti, S., G. Pagnoni, and F. Zaniboni (2006). "The landslides and tsunamis of the 30th of December 2002 in Stromboli analysed through numerical simulations". *Bulletin of Volcanology* 68(5), pages 462–479. DOI: 10.1007/s00445-005-0022-9.

Truswell, E., P. Quilty, A. McMinn, M. Macphail, and G. Wheeler (2005). "Late Miocene vegetation and palaeoenvironments of the Drygalski Formation, Heard Island, Indian Ocean: evidence from palynology". *Antarctic Science* 17(3), pages 427–442. DOI: 10.1017/s0954102005002865.

Urlaub, M., P. J. Talling, and D. G. Masson (2013). "Timing and frequency of large submarine landslides: implications for understanding triggers and future geohazard". *Quaternary Science Reviews* 72, pages 63–82. DOI: 10.1016/j.quascirev.2013.04.020.

Van Vliet-Lanoë, B., F. Bergerat, P. Allemand, C. Innocentd, H. Guillou, T. Cavailhes, Á. Guðmundsson, G. Chazot, J.-L. Schneider, P. Grandjean, C. Liorzou, and S. Passot (2019). "Tectonism and volcanism enhanced by deglaciation events in southern Iceland". *Quaternary Research* 94, pages 94–120. DOI: 10.1017/qua.2019.68.

Van Wyk de Vries, B., N. Kerle, and D. Petley (2000). "Sector collapse forming at Casita volcano, Nicaragua". *Geology* 28(2), page 167. DOI: 10.1130/0091-7613(2000)28<167:scfacv>2.0.co;2.

Walbridge, S., N. Slocum, M. Pobuda, and D. Wright (2018). "Unified Geomorphological Analysis Workflows with Benthic Terrain Modeler". *Geosciences* 8(3), page 94. DOI: 10.3390/geosciences8030094.

Watt, S. F. L. (2019). "The evolution of volcanic systems following sector collapse". *Journal of Volcanology and Geothermal Research* 384, pages 280–303. DOI: 10.1016/j.jvolgeores.2019.05.012.

Watt, S. F. L., J. Karstens, and C. Berndt (2021). "Volcanic-Island Lateral Collapses and Their Submarine Deposits". *Volcanic Debris Avalanches*. Edited by M. Roverato, A. Dufresne, and J. Procter. Springer International Publishing, pages 255–279. ISBN: 9783030574116. DOI: 10.1007/978-3-030-57411-6_10.

Watt, S. F. L., D. M. Pyle, and T. A. Mather (2013). "The volcanic response to deglaciation: Evidence from glaciated arcs and a reassessment of global eruption records". *Earth-Science Reviews* 122, pages 77–102. DOI: 10.1016/j.earscirev.2013.03.007.

Wilson, A. and J. Russell (2020). "Glacial pumping of a magma-charged lithosphere: A model for glaciovolcanic causality in magmatic arcs". *Earth and Planetary Science Letters* 548, page 116500. DOI: 10.1016/j.epsl.2020.116500.

Woodhead, J. (2002). "A simple method for obtaining highly accurate Pb isotope data by MC-ICP-MS". *Journal of Analytical Atomic Spectrometry* 17(10), pages 1381–1385. DOI: 10.1039/b205045e.

Yamazaki, Y., T. Lay, and K. F. Cheung (2021). "A Compound Faulting Model for the 1975 Kalapana, Hawaii, Earthquake, Landslide, and Tsunami". *Journal of Geophysical Research: Solid Earth* 126(11). DOI: 10.1029/2021jb022488.

York, D. (1968). "Least squares fitting of a straight line with correlated errors". *Earth and Planetary Science Letters* 5, pages 320–324. DOI: 10.1016/s0012-821x(68)80059-7.

Zernack, A. (2021). "Volcanic Debris-Avalanche Deposits in the Context of Volcaniclastic Ring Plain Successions—A Case Study from Mt. Taranaki". *Volcanic Debris Avalanches*. Edited by M. Roverato, A. Dufresne, and J. Procter. Springer International Publishing, pages 211–254. ISBN: 9783030574116. DOI: 10.1007/978-3-030-57411-6_9.